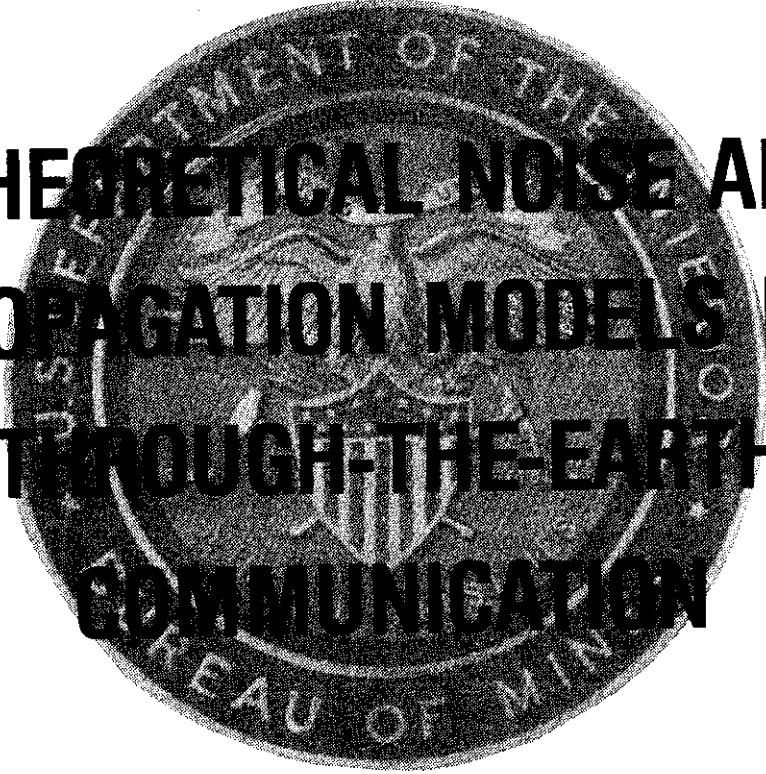


A minerals research contract report  
May 1982

82



**THEORETICAL NOISE AND  
PROPAGATION MODELS FOR  
THROUGH-THE-EARTH  
COMMUNICATION**

Contract J0113058  
National Telecommunications and  
Information Administration  
Institute for Telecommunication Sciences

*Lithology of the ... The views and conclusions contained in this document are those of the authors and should not be interpreted as necessarily representing the official policies or recommendations of the Interior Department's Bureau of Mines or of the U.S. Government.*

The views and conclusions contained in this document are those of the authors and should not be interpreted as necessarily representing the official policies or recommendations of the Interior Department's Bureau of Mines or of the U.S. Government.

REPORT DOCUMENTATION PAGE	1. REPORT NO.	2.	3. Recipient's Accession No.
4. Title and Subtitle Theoretical Noise and Propagation Models for Through-the-earth Communication		5. Report Date May 1982	
7. Author(s) D.A. Hill and J.R. Wait		6.	
9. Performing Organization Name and Address National Telecommunications & Information Admin. Institute for Telecommunication Sciences 325 Broadway Boulder, CO 80303		8. Performing Organization Rept. No.	
12. Sponsoring Organization Name and Address U.S. Dept. of the Interior Bureau of Mines 2401 E. Street, N.W. Washington, D.C. 20241		10. Project/Task/Work Unit No.	
15. Supplementary Notes		11. Contract(C) or Grant(G) No. (C) J0113058 (G)	
16. Abstract (Limit: 200 words) A survey of the literature on ELF and VLF atmospheric noise has been made. Most measurements have concentrated on the vertical electric field and the horizontal magnetic field rather than the vertical magnetic field which is of interest in transmission between horizontal loops. The limited vertical magnetic field data indicates that the vertical component is generally 10 to 20 dB below the horizontal component.  Three laterally inhomogeneous earth models have been analyzed for conversion of horizontal to vertical magnetic field. The rough surface model examines surface effects, the inhomogeneous thin sheet model treats volume effects, and the buried cylinder model treats localized man-made effects. All three models predict the possibility of significant conversion from horizontal to vertical magnetic field.  A thin sheet model has also been used to examine transmission from a buried magnetic dipole source. It it found that the predicted fields (con't below)		13. Type of Report & Period Covered Final 6/1/81-5/31/82	
17. Document Analysis a. Descriptors more nearly model the measured data than does the homogeneous half-space model.  b. Identifiers/Open-Ended Terms Atmospheric noise; conductivity; mine communication; vertical magnetic dipole; vertical magnetic field.  c. COSATI Field/Group		14.	
18. Availability Statement Release Unlimited		19. Security Class (This Report) Unclassified	21. No. of Pages 45
		20. Security Class (This Page) Unclassified	22. Price

## TABLE OF CONTENTS

	Page
ABSTRACT	1
1. INTRODUCTION	1
2. REVIEW OF ELF AND VLF NOISE	2
2.1 Introduction	2
2.2 Atmospheric Noise	3
2.3 Vertical Magnetic Noise	5
3. ROUGH SURFACE SCATTERING	6
3.1 Introduction	6
3.2 Formulation	6
3.3 Perturbation Solution	9
3.4 Quasi-static Approximation	12
3.5 Conclusions	14
4. SCATTERING BY AN INHOMOGENEOUS THIN SHEET	14
4.1 Introduction	14
4.2 Formulation	15
4.3 Solution for $c_n$	18
4.4 Vertical Magnetic Field	21
4.5 Surface Impedance	24
4.6 Conclusions	24
5. SCATTERING BY A BURIED CLYINDER	25
5.1 Introduction	25
5.2 Formulation for the Fields	25
5.3 Derivation of the Cylinder Current	27
5.4 Numerical Results	28
5.5 Conclusions	28
6. EFFECT OF A THIN CONDUCTING SHEET ON THE FIELDS OF A BURIED MAGNETIC DIPOLE	32
6.1 Introduction	32
6.2 Formulation	33
6.3 Vertical Magnetic Field in Air	35
6.4 Apparent Earth Conductivity	36
6.5 Conclusions	40
7. CONCLUSIONS AND RECOMMENDATIONS	41
8. REFERENCES	42

## FOREWORD

This report was prepared by the National Telecommunications and Information Administration, Institute for Telecommunication Sciences, Systems Technology and Standards Division, Boulder, Colorado 80303 under USBM Contract Number J0113058. The contract was initiated under the Minerals Health and Safety Technology Program. It was administered under the technical direction of U.S. Bureau of Mines with John Durkin acting as Technical Project Officer. A.G. Young was the contract administrator for the Bureau of Mines. This report is a summary of the work recently completed as a part of this contract during the period June 1, 1981 to May 31, 1982. This report was submitted by the authors on May 3, 1982.

THEORETICAL NOISE AND PROPAGATION MODELS  
FOR THROUGH-THE-EARTH COMMUNICATION

D. A. Hill\* and J. R. Wait\*\*

ABSTRACT

A survey of the literature on ELF and VLF atmospheric noise has been made. Most measurements have concentrated on the vertical electric field and the horizontal magnetic field rather than the vertical magnetic field which is of interest in transmission between horizontal loops. The limited vertical magnetic field data indicates that the vertical component is generally 10 to 20 dB below the horizontal component.

Three laterally inhomogeneous earth models have been analyzed for conversion of horizontal to vertical magnetic field. The rough surface model examines surface effects, the inhomogeneous thin sheet model treats volume effects, and the buried cylinder model treats localized man-made effects. All three models predict the possibility of significant conversion from horizontal to vertical magnetic field.

A thin sheet model has also been used to examine transmission from a buried magnetic dipole source. It is found that the predicted fields more nearly model the measured data than does the homogeneous half-space model.

Key Words: Atmospheric noise; conductivity; mine communication; vertical magnetic dipole; vertical magnetic field.

1. INTRODUCTION

During the past decade, a great deal of theoretical and experimental research has been conducted on communication with miners trapped within the mine workings. Numerous antenna configurations and earth conductivity models have been proposed and analyzed. Many of the results are contained in a recent summary report (Wait and Hill, 1980a). Also, the systems aspects of electromagnetic detection of trapped miners have recently been studied (Lagace, et al., 1980).

A weakness in attempting to compute detection probabilities for trapped miners using horizontal loop antennas is the lack of a good data base for

\* The author is with the Institute for Telecommunication Sciences, National Telecommunications and Information Administration, U.S. Department of Commerce, Boulder, Colorado 80303.

\*\*The Author is with the Department of Electrical Engineering, University of Arizona, Tucson, Arizona 85721, and is a consultant to NTIA/ITS, Boulder, Colorado 80303.

magnetic noise for the low frequencies (ELF and VLF) which are required in transmission through the earth (Lagace, et al., 1980). The primary purposes of this report are to review the current state of knowledge of magnetic noise at ELF and VLF and to examine theoretical models for the vertical component of magnetic noise. Indeed, it is the vertical component of magnetic noise which is the interfering component in transmission between horizontal loops.

Our secondary objective is to analyze earth conductivity models in order to explain some trends in measured data for transmission between horizontal loops. An analysis of transmission data gathered at numerous coal mines has indicated that the usual homogeneous half-space model for the earth is inadequate for explaining the depth and frequency dependence of transmission loss (Durkin, 1981).

The organization of this report is as follows: In Section 2, the past work on ELF and VLF noise is reviewed with an emphasis on atmospheric noise. A lack of measured data underlies the need for more measurements and a better understanding of vertical magnetic noise. Sections 3-5 analyze three laterally inhomogeneous earth models and the generation of vertical magnetic noise from the dominant horizontal component. Section 3 analyzes rough surface scattering and includes the effect of finite earth conductivity. Section 4 analyzes an inhomogeneous thin conducting layer which is representative of volume scattering effects. Section 5 analyzes scattering by a buried cylinder which could represent a buried pipe, rail, or wire. In Section 6, the effect of a thin surface layer of high conductivity on the surface fields of a buried horizontal loop are analyzed and compared with measured data from coal mines. Finally, Section 7 contains the overall conclusions and recommendations.

## 2. REVIEW OF ELF AND VLF NOISE

### 2.1 Introduction

The range of frequencies of interest in through-the-earth detection of and communication with trapped miners is roughly from 10 Hz to 6 kHz. Thus both the ELF (3 Hz - 3 kHz) and VLF (3 kHz - 30 kHz) bands are included. Also both surface and subsurface noise are important because both uplink and downlink transmission are desirable. Although many noise measurements reported in the

literature have been made with vertical whips to obtain the vertical electric field in air, we are interested in magnetic noise for loop-to-loop applications.

During the 1970's, the National Bureau of Standards made wideband noise measurements both within and above numerous coal mines (Bensema, 1972; Bensema, 1977). The majority of these measurements were made under operational conditions, and man-made noise was generally dominant. Two of the prominent features of man-made noise in an operational mine are the 60 Hz harmonics from power lines and wideband impulses from machinery. For mine rescue situations, the mine will be shut down, and a narrow-band signal located between the 60 Hz harmonics will be transmitted (Lagace, et al., 1980). Consequently, man-made noise is not expected to be significant and will not be discussed further here. Atmospheric noise from lightning is the dominant interferer and will be discussed in detail in the following section.

## 2.2 Atmospheric Noise

Atmospheric noise produced by lightning can usually be split into near-field noise from local thunderstorms and background noise from distant thunderstorms which propagates via the earth-ionosphere waveguide. A good description of the characteristics of lightning and atmospheric noise is given by A. D. Watt in Chapter 5 of his book on VLF Radio Engineering (Watt, 1967). The noise from local thunderstorms tends to be randomly polarized and highly impulsive. Since search operations would probably be temporarily halted during periods of high noise activity from local storms (Lagace, et al., 1980), we will consider here only atmospheric noise from distant thunderstorms.

The most extensive reference on atmospheric radio noise is probably CCIR Report 322 (1964). It contains worldwide contour maps of atmospheric noise levels at 1 MHz for 4-hour intervals for 3-month periods. The maps are in local time, and 24 maps are required to cover the 6 time blocks and 4 seasons. With each map curves of frequency dependence are given, but the lower limit of each curve is 10 kHz. Thus the maps are not directly useful for our frequency range. However, Stone and Maxwell (1965), have generated worldwide noise maps in Universal Time for 10 kHz from CCIR Report 322. Again 24 maps are given to cover the 6 time blocks and 4 seasons. Watt has also reproduced the same maps in Chapter 5 of VLF Radio Engineering, (1967). In addition Watt (1967) has



published frequency dependence curves for the range from 1 kHz to 100 kHz. Thus the 10 kHz maps can be extrapolated downward to cover much of our frequency range. Watt (1967) has also published curves of the upper decile, i.e., the noise value which is exceeded 10% of the time, for the four seasons for frequencies from 1 kHz to 100 kHz.

Although the 10 kHz maps of Maxwell and Stone (1965) are still the best VLF atmospheric noise maps available, they suffer from the weaknesses that they are primarily obtained by downward extrapolation in frequency and they do not account for the known non-reciprocal earth-ionosphere waveguide attenuation rates. In addition, it is necessary to do further extrapolation downward in frequency from the curves of Watt (1967) to reach our frequency range (below 6 kHz). Fortunately there were some atmospheric noise measurements at ELF performed during the 1960's and the 1970's because of the interest in long distance communication to submarines for Project Sanguine (later Seafarer). A special issue of the IEEE Transactions on Communications was devoted to ELF communications and, Project Sanguine in 1974 (Wait, 1974), and it contains several references to ELF noise. Earlier measurements and noise curves were also given by Maxwell and Stone (1963) and Maxwell (1967). The measurements of vertical electric field with vertical whips and horizontal magnetic field with vertical loops indicated that the E/H ratio was approximately that of free space (377 ohms) except between 1 kHz and 5 kHz where the ratio is somewhat greater. The region between 1 kHz and 5 kHz is where the dominant earth-ionosphere waveguide mode switches from the TEM (transverse electromagnetic) mode at ELF to the first order TM (transverse magnetic) mode at VLF (Watt, 1967; Wait, 1962). A result of this transition is that the overall attenuation reaches a peak and the atmospheric noise is at a minimum in the vicinity of 2 kHz (Maxwell, 1967).

A recent review of ELF noise by Soderberg (1981) gives an extensive bibliography and lists presently active ground stations with capability for measurement of ELF noise. Most published data of ELF or VLF atmospheric noise give either the vertical electric field or the horizontal magnetic field because they are the dominant components of both the TEM or the first order TM modes in the earth-ionosphere waveguide (Wait, 1962). The vertical magnetic field which is of interest in our application will be discussed in the following section.

### 2.3 Vertical Magnetic Noise

Although most magnetic noise measurements have considered only the horizontal component, the National Bureau of Standards (Adams, et al., 1974) and the U. S. Bureau of Mines (Lagace, et al., 1980) have made some measurements of the vertical component using horizontal loops. The National Bureau of Standards (Adams, et al., 1974) measured both horizontal and vertical magnetic noise in a remote area in Utah with no power lines in the vicinity, and they were able to observe strong atmospheric noise above the cutoff of the first order TM mode. The cutoff frequency was approximately 1.7 kHz at night and 3.5 kHz during the day. The vertical component tended to be 10 to 15 dB below the horizontal component which is consistent with earlier dip angle measurements by Ward, et al. (1966). The U.S. Bureau of Mines measured vertical magnetic noise at four frequencies, 630, 1050, 1950, and 3030 Hz, above 27 mines, and the findings are summarized in (Lagace, et al., 1980). The general trends are in agreement with the published data on horizontal magnetic atmospheric noise, but the levels are lower. Further magnetic noise measurements are proceeding in order to learn more about the relationship of vertical to horizontal noise and the depth dependence which is important in downlink transmission.

Although the vertical magnetic field is not normally measured in the magneto-telluric method of geophysical prospecting (Keller and Frischknecht, 1966), the presence of a vertical magnetic field has been noted as an indicator of lateral variation in earth conductivity (Sims and Bostick, 1969; Word, et al., 1970). At frequencies above 1 Hz, thunderstorms are the primary source of energy used in magneto-tellurics (Keller and Frischknecht, 1966). It is only below 1 Hz that micropulsations of the earth's magnetic field account for the magneto-telluric field.

A general analysis of inhomogeneous earth models is very complicated (Word, et al., 1970), but the physics of the generation of vertical magnetic noise can be understood from fairly simple models. In Sections 3-5, we analyze three cases of generation of vertical magnetic noise by inhomogeneous earth models. In each case we make the following simplifying assumptions which are commonly made in magneto-tellurics (Keller and Frischknecht, 1966): (1) for a given spectral component, that varies as  $e^{i\omega t}$ , the exciting field is spatially uniform and linearly polarized, (2) earth curvature is neglected, and (3) the

earth conductivity varies only in the vertical and one horizontal direction. Specifically we assume that the incident field has only a y-directed electric field  $E_y$  and an x-directed magnetic field  $H_x$  and that the earth conductivity is invariant in the y direction. Thus we can treat two-dimensional geometries with E-polarization for which only  $E_y$ ,  $H_x$ , and  $H_z$  are nonzero. The vertical magnetic field  $H_z$  is a consequence of lateral variation of earth conductivity and would be zero for a simple horizontally-stratified earth. Actually an H-polarized solution with  $H_y$ ,  $E_x$ , and  $E_z$  is also possible, but is not of interest to us in this report because it does not contain a vertical magnetic field component. In sections 3-5, we will be particularly interested in the ratio of  $H_z$  to  $H_x$  and the spatial and frequency dependence of  $H_z$ .

### 3. ROUGH SURFACE SCATTERING

#### 3.1 Introduction

In this section we consider a conducting earth model where the earth is homogeneous, but the air-earth interface is slightly rough. Our perturbation analysis is similar to earlier analyses of periodic sea waves (Barrick, 1971; Wait, 1971b; Rosich and Wait, 1977), but here we treat the finite conductivity of the earth directly rather than employing the impedance boundary condition. In this way we are able to examine the fields in the earth which are relevant to the downlink communication application.

We make the usual magneto-telluric assumption that the incident field is a plane wave at normal incidence (Mann, 1964), and we assume that the surface is periodic and two-dimensional. Also we treat only electric polarization ( $E_y$ ,  $H_x$ , and  $H_z$  are nonzero) because we are primarily interested in the generation of the vertical magnetic field ( $H_z$ ) by rough surface scattering.

#### 3.2 Formulation

The geometry of the two-dimensional surface is shown in Figure 1. Initially the surface,  $z = s(x)$ , is periodic with period  $L$ , and  $s(x)$  can be written as a Fourier series

$$s(x) = \sum_m P_m e^{-i2\pi mx/L}, \quad (1)$$

where  $P_0 = 0$  and  $P_m = P_{-m}^*$  for a real surface with zero mean height. The region  $z < s(x)$  is free space with permittivity  $\epsilon_0$ , and the region  $z > s(x)$  is earth with permittivity  $\epsilon$  and conductivity  $\sigma$ . Free space permeability  $\mu_0$  is assumed everywhere.

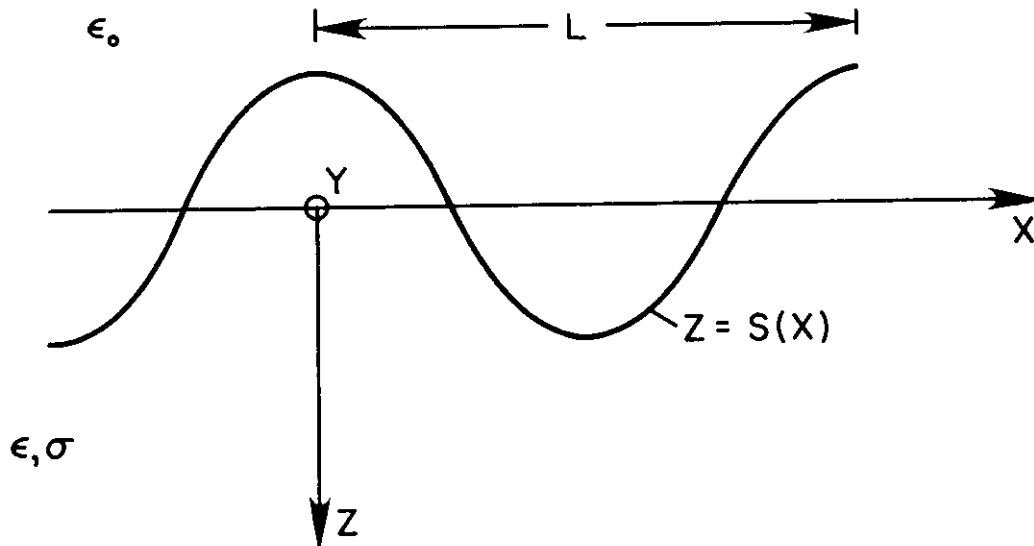


Figure 1. Geometry of the two-dimensional periodic rough surface,  $z = s(x)$ .

The electric field in free space  $E_{oy}$  can be written as a discrete spectrum of plane waves:

$$E_{oy} = e^{-\gamma_0 z} + \sum_m a_m e^{\gamma_0 C_m z - i2\pi mx/L}, \quad (2)$$

where  $\gamma_0 = i\omega(\mu_0 \epsilon_0)^{1/2}$ ,  $C_m = \left[ 1 + \left( \frac{2\pi m}{\gamma_0 L} \right)^2 \right]^{1/2}$ ,

and  $\exp(i\omega t)$  time dependence is assumed. The term  $\exp(-\gamma_0 z)$  is the incident plane wave normalized to unit magnitude and the summation is the discrete spectrum of plane waves where the amplitudes  $a_m$  are unknown at this point.  $C_m$  is chosen so that  $E_{oy}$  satisfies the scalar Helmholtz equation

$$(\nabla^2 - \gamma_0^2) E_{oy} = 0 \quad (3)$$

The magnetic field components in free space,  $H_{ox}$  and  $H_{oz}$ , are obtained from  $E_{oy}$  by Maxwell's curl equation

$$H_{ox} = \frac{1}{i\omega\mu_0} \frac{\partial E_{oy}}{\partial z} \quad \text{and} \quad H_{oz} = \frac{-1}{i\omega\mu_0} \frac{\partial E_{oy}}{\partial x} \quad (4)$$

The electric field in the earth  $E_y$  is written as a discrete sum of transmitted plane waves

$$E_y = \sum_m b_m e^{-\gamma D_m z - i2\pi m x/L} \quad (5)$$

where  $\gamma = [i\omega\mu_0(\sigma + i\omega\epsilon)]^{1/2}$ ,  $D_m = \left[ 1 + \left( \frac{2\pi m}{\gamma L} \right)^2 \right]^{1/2}$ ,

and amplitudes  $b_m$  are unknown. Again  $D_m$  is chosen so that  $E_y$  satisfies the scalar Helmholtz equation

$$(\nabla^2 - \gamma^2) E_y = 0 \quad (6)$$

The magnetic field components in the earth,  $H_x$  and  $H_z$ , are given by

$$H_x = \frac{1}{i\omega\mu_0} \frac{\partial E_y}{\partial z} \quad \text{and} \quad H_z = \frac{-1}{i\omega\mu_0} \frac{\partial E_y}{\partial x} \quad (7)$$

In writing (2) and (5), we are invoking the Rayleigh hypothesis (Strutt, 1896) which states that only outgoing waves are needed in the trough regions. According to Millar (1971), this is valid for sinusoidal surfaces when the slope is less than .448 everywhere. This is not a significant limitation for our perturbation method which assumes small slope.

The boundary conditions, imposed at the surface  $z = s(x)$ , are that the tangential electric and magnetic fields are continuous across the interface

$$E_{oy} \Big|_{z=s(x)} = E_y \Big|_{z=s(x)} \quad (8)$$

and

$$\frac{H_{ox} + H_{oz} \frac{ds}{dx}}{\left[1 + \left(\frac{ds}{dx}\right)^2\right]^{1/2}} \Big|_{z=s(x)} = \frac{H_x + H_z \frac{ds}{dx}}{\left[1 + \left(\frac{ds}{dx}\right)^2\right]^{1/2}} \Big|_{z=s(x)} \quad (9)$$

By substituting (2) and (5) into (8) and (4) into (9), the following expressions are obtained

$$e^{-\gamma_o s} + \sum_m (a_m e^{\gamma_o C_m s} - b_m e^{-\gamma D_m s}) e^{-i2\pi m x/L} = 0 \quad (10)$$

and

$$\begin{aligned} & \frac{-e^{-\gamma_o s}}{\eta_o} + \sum_m a_m \left( \frac{C_m}{\eta_o} + \frac{2\pi m}{\omega \mu_o L} \frac{ds}{dx} \right) e^{\gamma_o C_m s - i2\pi m x/L} \\ & = \sum_m b_m \left( \frac{-D_m}{\eta} + \frac{2\pi m}{\omega \mu_o L} \frac{ds}{dx} \right) e^{-\gamma C_m s - i2\pi m x/L} \end{aligned} \quad (11)$$

where  $\eta_o = (\mu_o/\epsilon_o)^{1/2}$

and  $\eta = \left( \frac{\sigma + i\omega\epsilon}{i\omega\mu_o} \right)^{1/2}$ .

In obtaining (11), we have canceled the square root denominators in (9).

### 3.3 Perturbation Solution

In general the solution of (10) and (11) for  $a_m$  and  $b_m$  must be obtained numerically (Chuang and Kong, 1981), but for sufficiently small surface slope and height we can utilize a perturbation solution (Barrick, 1971; Wait, 1971; Rosich and Wait, 1977; Mann, 1964; Strutt, 1896). Specifically, we assume

that  $ds/dx$ ,  $\gamma_o s$ , and  $\gamma s$  are small first-order quantities. The unknowns  $a_m$  and  $b_m$  are expanded in a perturbation series to first-order

$$a_m \approx a_m^{(0)} + a_m^{(1)} + \dots$$

and

$$b_m \approx b_m^{(0)} + b_m^{(1)} + \dots \quad (12)$$

The perturbation series in (12) could be carried to any arbitrary order (Rosich and Wait, 1977), but a first-order result is sufficient to yield information concerning the vertical magnetic field.

If we substitute (12) into (10) and (11) and expand the exponential factors involving  $s$  in a power series, then we can equate zero order quantities to obtain

$$a_o^{(0)} = \frac{\gamma_o - \gamma}{\gamma_o + \gamma}, \quad b_o = \frac{2\gamma_o}{\gamma_o + \gamma}, \quad (13)$$

and  $a_o^{(0)} = b_m^{(0)} = 0$  for  $m \neq 0$ .

The results in (13) are simply the plane wave reflection and transmission coefficients for a planar interface. Substitution of (13) into (2), (4), (5), and (7) yields the zero-order plane wave fields

$$\begin{aligned} E_{oy}^{(0)} &= e^{-\gamma_o z} + a_o^{(0)} e^{\gamma_o z}, \\ H_{ox}^{(0)} &= \frac{1}{\eta_o} (-e^{-\gamma_o z} + a_o^{(0)} e^{\gamma_o z}), \end{aligned} \quad (14)$$

$$\begin{aligned} E_y^{(0)} &= b_o^{(0)} e^{-\gamma z}, \\ \text{and } H_x^{(0)} &= \frac{-b_o^{(0)}}{\eta} e^{-\gamma z}. \end{aligned}$$

Note that the zero-order solution does not generate any vertical magnetic field

$$H_{oz}^{(0)} = H_z^{(0)} = 0. \quad (15)$$

By equating first-order terms in the expansions of (10) and (11), we obtain

$$a_m^{(1)} = b_m^{(1)} = \frac{(\gamma_o^2 - \gamma^2) b_o^{(0)}}{\gamma_o C_m + \gamma D_m} P_m \quad (16)$$

which agrees with an earlier result of Rice (1951). An interesting special case is to let the surface be a pure cosine of height D

$$s(x) = D \cos \left( \frac{2\pi x}{L} \right) \quad (17)$$

Then the Fourier coefficients in (1) are

$$P_1 = P_{-1} = D/2 \quad (18)$$

and  $P_m = 0$  for  $m \neq \pm 1$ .

Then (16) reduces to

$$a_{\pm 1}^{(1)} = b_{\pm 1}^{(1)} = \frac{(\gamma_o^2 + \gamma^2) b_o^{(0)} D}{2(\gamma_o C_1 + \gamma D_1)} \quad (18)$$

and  $a_m^{(1)} = b_m^{(1)} = 0$  for  $m \neq \pm 1$ .

From (4), (7), and (18), the first-order vertical magnetic field components,  $H_{oz}^{(1)}$  and  $H_z^{(1)}$ , are given by

$$\left. \begin{array}{l} H_{oz}^{(1)} \\ H_z^{(1)} \end{array} \right\} = \frac{2a_1^{(1)}}{i\omega\mu_o} (2\pi/L) \sin(2\pi x/L) \cdot \left\{ \begin{array}{l} e^{\gamma_o C_1 z} \\ e^{-\gamma D_1 z} \end{array} \right. \quad (19)$$

The factor,  $\sin(2\pi x/L)$ , in (19) indicates that the first-order vertical magnetic field is proportional to the surface slope  $ds/dx$ .



### 3.4 Quasi-static Approximation

In the frequency range of interest here (ELF and VLF), the following approximations are valid

$$|\gamma/\gamma_0| \gg 1 \text{ and } \gamma \approx (i\omega\mu_0\sigma)^{1/2} . \quad (20)$$

By substituting (20) and (13) into (14), we obtain the zero order magnetic field

$$H_{ox}^{(0)} \approx \frac{-1}{\eta_0} (e^{-\gamma_0 z} + e^{\gamma_0 z})$$

and

$$H_x^{(0)} \approx \frac{-2}{\eta_0} e^{-\gamma z} .$$

Thus the zero-order magnetic field at  $z = 0$  is twice the incident field, and we define it according to

$$H_0 \equiv -2/\eta_0 . \quad (22)$$

By substituting (20) and (22) into (19), we obtain the quasi-static approximation for the vertical magnetic field

$$\left. \begin{array}{l} H_{oz}^{(1)} \\ H_z^{(1)} \end{array} \right\} \approx H_0 \left[ -\frac{2\pi D}{L} \sin\left(\frac{2\pi x}{L}\right) \right] F(\gamma L) \cdot \left\{ \begin{array}{l} e^{\gamma_0 C_1 z} \\ e^{-\gamma D_1 z} \end{array} \right. , \quad (23)$$

where

$$F(\gamma L) = \frac{1}{\left[ 1 + (2\pi/\gamma L)^2 \right]^{1/2} + \frac{2\pi}{\gamma L}} . \quad (24)$$

The vertical magnetic field expression in (23) has a simple interpretation.  $H_0$  is the zero-order horizontal magnetic field at the interface. The factor,  $-(2\pi D/L)\sin(2\pi x/L)$ , is the slope of the surface,  $ds/dx$ . The exponential factors account for the propagation of the  $m = 1$  mode away from the interface and are

approximately equal to unity for small  $|z|$ . The factor  $F(\gamma L)$  accounts for the imperfect conductivity of the earth. For large  $|\gamma|L$  (perfect conductivity),  $F(\gamma L) \approx 1$ . For small  $|\gamma|L$  (poor conductivity),  $F(\gamma L) \approx 0$ .

The dependence of the magnitude and phase of  $F$  on  $|\gamma|L$  is shown in Figure 2. It is readily seen that  $|\gamma|L$  must be quite large before  $F$  approaches unity. To consider some typical parameters, let  $f = 1$  kHz,  $\sigma = 10^{-2}$  S/m, and  $L = 1$  km. Then  $|\gamma|L \approx 8.9$ , and from Figure 2,  $|F| \approx 0.59$ .

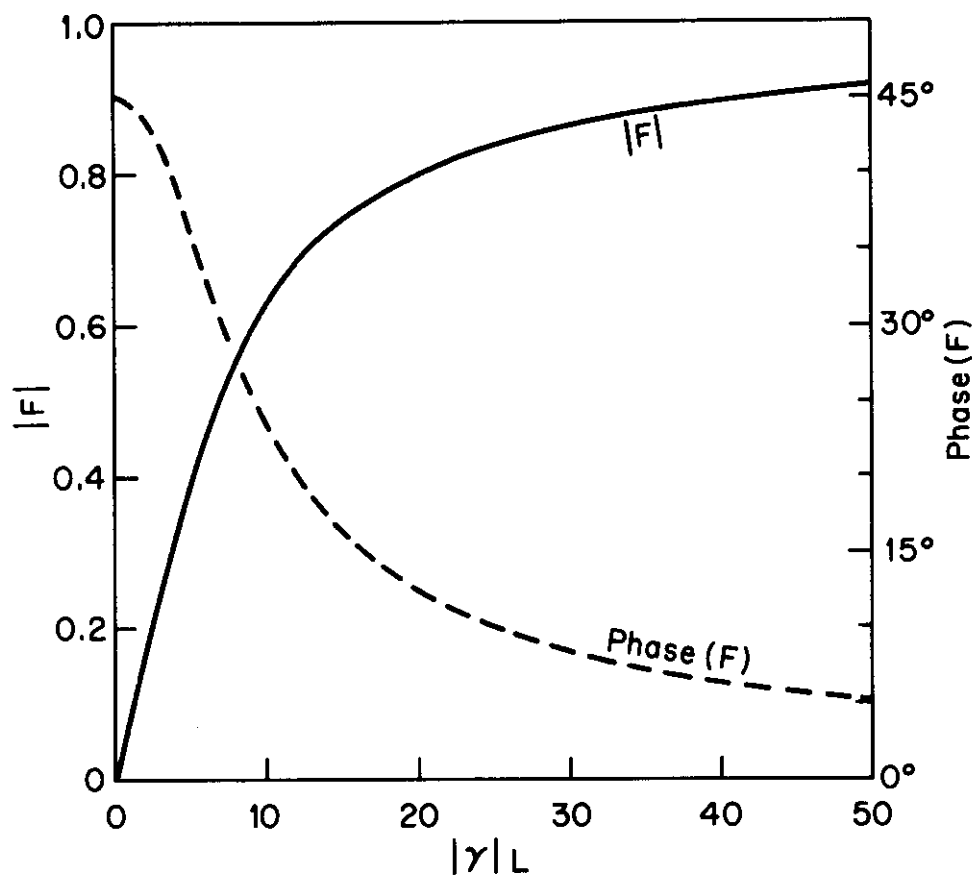


Figure 2. Magnitude and phase of  $F$  as a function of  $|\gamma|L$ .

As a check for perfect conductivity, when  $z$  is small (23) can be written

$$H_{oz}^{(1)} \approx H_o \frac{ds}{dx} \quad (25)$$

When this is combined with the zero order magnetic field in (21), the result is that the normal component of magnetic field is zero at the surface. This is a

required boundary condition for a perfect conductor, and it agrees with Ishimaru's result (Ishimaru, 1978) for a perfectly conducting rough surface.

### 3.5 Conclusions

We have derived a first order result for the fields in the presence of a two-dimensional rough surface. The vertical magnetic field has been examined in detail and is found to have a simple physical interpretation. For a perfectly conducting earth, the vertical magnetic field is proportional to the surface slope times the unperturbed horizontal magnetic field. The effect of finite conductivity is a reduction by the simple factor  $F(\gamma L)$  as given by (24).

Only the cosine surface was considered in detail here, but the general result in (16) for arbitrary Fourier coefficients would allow the treatment of arbitrary surface profiles by superposition. Hughes and Wait (1975) have treated a two-layer earth with an arbitrary interface profile by perturbation. Also we could extend our treatment to arbitrary incidence in the y-z plane, but then the solution becomes more complicated because the E- and H- polarizations are coupled.

## 4. SCATTERING BY AN INHOMOGENEOUS THIN SHEET

### 4.1 Introduction

In the previous section we examined the generation of the vertical magnetic field by surface roughness. In this section we analyze a simple model which illustrates the effect of volume irregularities. The model consists of a thin conducting sheet at an arbitrary depth in an otherwise homogeneous half space. The conductivity-thickness product of the thin sheet is allowed to vary in the x direction as indicated in Figure 3. Since the structure is invariant in the y direction, we have a two-dimensional problem with two possible polarizations. Only the electric polarization is of interest here, and the nonzero field components are  $E_y$ ,  $H_x$ , and  $H_z$ .

To simplify the problem even further, we assume that the tangential magnetic field at the interface is a constant.

$$H_x \Big|_{z=0} = H_0. \quad (26)$$

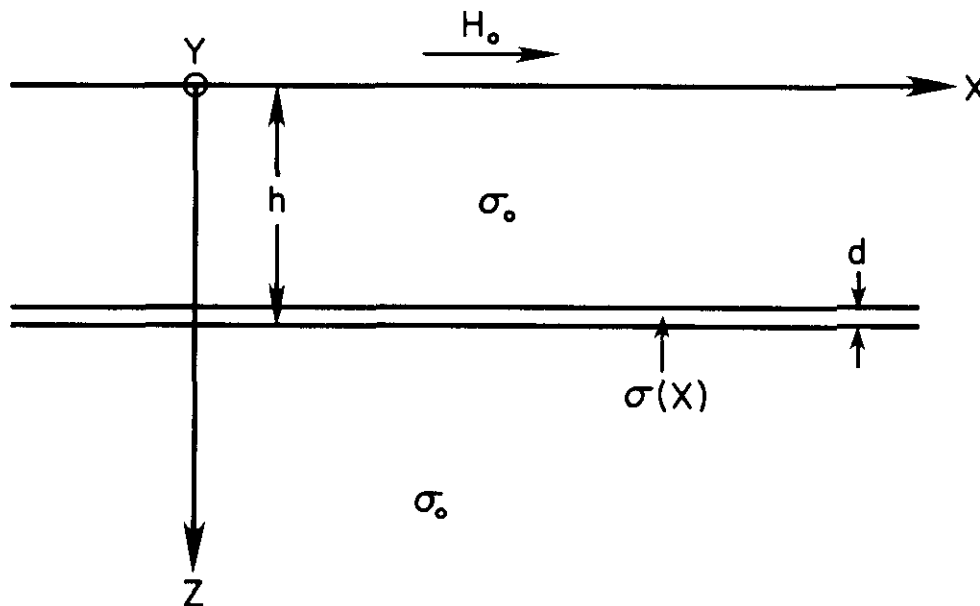


Figure 3. Geometry for a thin conducting sheet in a homogeneous half space.

The constant magnetic field assumption is frequently made in magneto-telluric problems (Rankin, 1962; Geyer, 1972; Reddy and Rankin, 1973; Wait and Spies, 1974), and the validity of this assumption has recently been examined by Hohman (1981). The primary advantage of the assumption is that only the fields in the earth ( $z > 0$ ) need to be considered. However, the model yields information on the fields at the surface in air because of the required continuity at the earth surface.

#### 4.2 Formulation

The geometry of the conducting half space is shown in Figure 3. The conductivity of the half space is  $\sigma_0$ , and the conducting sheet of thickness  $d$  is located at a depth  $h$ . The sheet conductivity  $\sigma(x)$  is taken to have the periodic form

$$\sigma(x) = \sigma + \Delta \cos\beta x \quad , \quad (27)$$

where  $\beta = 2\pi/L$  and  $L$  is the period. Free space permeability  $\mu_0$  is assumed everywhere, and  $d$  is assumed to be small compared to the layer skin depth.

The  $y$  component of electric field  $E_y$  satisfies the scalar Helmholtz equation

$$(\nabla^2 - \gamma^2)E_y = 0 \quad (28)$$

where  $\gamma = (i\omega\mu_0\sigma_0)^{1/2}$

and displacement currents are neglected. The magnetic field components  $H_x$  and  $H_y$  are derived from  $E_y$ :

$$H_x = \frac{1}{i\omega\mu_0} \frac{\partial E_y}{\partial z} \quad \text{and} \quad H_z = \frac{-1}{i\omega\mu_0} \frac{\partial E_y}{\partial x} \quad (29)$$

Given the periodicity of  $\sigma(x)$ , the fields are periodic in  $x$  and are of the general form  $\exp(+\Gamma_n z - i\beta nx)$ , where  $\Gamma_n = (\gamma^2 + \beta^2 n^2)^{1/2}$  with  $\text{Re}(\Gamma_n) > 0$ .

The fields above and below the thin sheet can be written in the specific form

$$\left. \begin{aligned} H_x &= \sum_n (a_n e^{-\Gamma_n z} + b_n e^{\Gamma_n z}) e^{-i\beta nx} \\ E_y &= -\sum_n K_n (a_n e^{-\Gamma_n z} - b_n e^{\Gamma_n z}) e^{-i\beta nx} \end{aligned} \right\} 0 < z < h \quad (30)$$

and

$$\left. \begin{aligned} H_x &= \sum_n c_n e^{-\Gamma_n z} e^{-i\beta nx} \\ E_y &= -\sum_n c_n e^{-\Gamma_n z} e^{-i\beta nx} \end{aligned} \right\} z > h \quad (31)$$

where  $K_n = i\omega\mu_0/\Gamma_n$ , the  $n$  summations are over all integers, and  $a_n$ ,  $b_n$ , and  $c_n$  are unknown coefficients. From the boundary condition on  $H_x$  at  $z = 0$  in (26) we obtain

$$a_n + b_n = H_o \delta_n \quad (32)$$

$$\text{where } \delta_n = \begin{cases} 1, & n = 0 \\ 0, & n \neq 0 \end{cases} .$$

Also the continuity of  $E_y$  at  $z = h$  yields

$$a_n e^{-\Gamma_n h} - b_n e^{\Gamma_n h} = c_n e^{-\Gamma_n h} . \quad (33)$$

From (32) and (33) we can solve for  $a_n$  and  $b_n$  in terms of  $c_n$ :

$$a_n = \frac{H_o \delta_n e^{2\Gamma_n h} + c_n}{1 + e^{2\Gamma_n h}} , \quad (34)$$

$$b_n = \frac{H_o \delta_n - c_n}{1 + e^{2\Gamma_n h}} .$$

The remaining boundary condition is that, in accordance with Ampere's law, the discontinuity in  $H_x$  at  $z = h$  is equal to the current density carried by the thin sheet:

$$H_x \Big|_{z=h^+} - H_x \Big|_{z=h^-} = d(\sigma + \Delta \cos \beta x) E_y \Big|_{z=h} \quad (35)$$

Substituting (30) and (31) into (35), we obtain

$$\begin{aligned} & - \sum_n [a_n e^{-\Gamma_n h} + b_n e^{\Gamma_n h} - c_n e^{-\Gamma_n h}] e^{-i\beta n x} \\ & = -d(\sigma + \Delta \cos \beta x) \sum_n K_n c_n e^{-\Gamma_n h} e^{-i\beta n x} . \end{aligned} \quad (36)$$

Using (34) and replacing  $\cos(\beta x)$  by its exponential form, we can rewrite (36):

$$\sum_n \left\{ \left[ c_n \left[ 1 - \left( \frac{1 - e^{-2\Gamma_n h}}{1 + e^{-2\Gamma_n h}} \right) + \sigma d K_n \right] - \frac{2H_o \delta_n e^{-2\Gamma_n h}}{1 + e^{-2\Gamma_n h}} \right] e^{-\Gamma_n h} + c_{n+1} \frac{\Delta d K_{n+1} e^{-\Gamma_{n+1} h}}{2} + c_{n-1} \frac{\Delta d K_{n-1} e^{-\Gamma_{n-1} h}}{2} \right\} \cdot e^{-i\beta n x} = 0 \quad (37)$$

Since (37) must be satisfied for all  $x$ , each Fourier coefficient must be zero:

$$c_n \left( \frac{2e^{-2\Gamma_n h}}{1 + e^{-2\Gamma_n h}} + \sigma d K_n \right) e^{-\Gamma_n h} + c_{n+1} \left( \frac{\Delta d}{2} K_{n+1} e^{-\Gamma_{n+1} h} \right) + c_{n-1} \left( \frac{\Delta d}{2} K_{n-1} e^{-\Gamma_{n-1} h} \right) = \frac{2H_o \delta_n e^{-\Gamma_n h}}{1 + e^{-2\Gamma_n h}} \quad (38)$$

From (38) it is seen that the effect of the  $x$  variation of  $\sigma(x)$  is to couple all of the  $c_n$  coefficients together and to introduce higher harmonics ( $n \neq 0$ ). For the special case of no  $x$  variation ( $\Delta=0$ ), (38) has a simple solution

$$c_n = \begin{cases} \frac{2H_o}{2 + (\sigma d K_o)(1 + e^{-2\gamma h})} & , n = 0 \\ 0, & n \neq 0 \end{cases} \quad (39)$$

In the following section, we examine the solution of (38) for  $\Delta \neq 0$ .

#### 4.3 Solution for $c_n$

For  $n \neq 0$ , we can write (38) in the following form

$$c_n \Omega_n + c_{n+1} P_{n+1} + c_{n-1} P_{n-1} = 0 \quad (40)$$

$$\text{where } \Omega_n = \left[ \frac{2}{1 + e^{-2\Gamma_n h}} + \sigma d K_n \right] e^{-\Gamma_n h}$$

$$\text{and } p_n = \frac{\Delta d}{2} K_n e^{-\Gamma_n h} .$$

We can rewrite (40) in the following form:

$$\frac{c_n}{c_{n-1}} = \frac{-p_{n-1}}{\Omega_n + p_{n+1} \frac{c_{n+1}}{c_n}} . \quad (41)$$

By incrementing  $n$  by unity, repeated use of (41) yields a continued fraction for  $c_n/c_{n-1}$ . In particular, for  $n = 1$  we have the following continued fraction

$$\frac{c_1}{c_0} = \frac{-p_0}{\Omega_1 + \frac{p_2(-p_1)}{\Omega_2 + \frac{p_3(-p_2)}{\Omega_3 + \frac{p_4(-p_3)}{\Omega_4 + \dots}}}} . \quad (42)$$

The continued fraction in (42) converges quite rapidly. Once  $c_1/c_0$  is computed from (42),  $c_0$  is computed from (38) for  $n = 0$ :

$$c_0 = \frac{2H_0}{1+e^{-2\gamma h}} \left\{ \frac{2}{1+e^{-2\gamma h}} + \sigma d K_0 + (c_1/c_0) \Delta d K_1 e^{-(\Gamma_1 - \gamma)h} \right\}^{-1} . \quad (43)$$

Then all higher order  $c_n$ 's can be computed from (40) by recurrence. Because of the symmetry of the geometry,  $c_{-n} = c_n$ , and only positive  $n$ 's need be considered.

The convergence of (42) is illustrated in Tables 1 and 2. The magnitude and phase of  $c_1/c_0$  are given as a function of  $N_T$ , the number of terms in the denominator of (42). Only a few terms are needed for convergence, and the convergence improves as  $h$  is increased. The value of  $\Delta d$  (1S) in Tables 1 and 2 is fairly large. For small values of  $\Delta d$ , the convergence is even faster and  $|c_1/c_0|$  is smaller.



TABLE 1. Magnitude of  $c_1/c_0$

$N_t \backslash h$	0	20m	50m	100m
1	0.6283	0.5794	0.5286	0.4898
2	0.5487	0.5279	0.4972	0.4695
3	0.5526	0.5295	0.4977	0.4698
4	0.5525	0.5295	0.4977	0.4698
5	0.5525	0.5295	0.4977	0.5698

$f = 1\text{kHz}$ ,  $\Delta d = 1\text{S}$ ,  $\sigma d = 0$ ,  $\sigma_o = 5 \times 10^{-3} \text{ S/m}$ ,  $L = 1\text{km}$ .

TABLE 2. Phase of  $c_1/c_0$

$N_T \backslash h$	0	20m	50m	100m
1	-135.0°	-139.6°	-145.0°	-150.5°
2	-131.0°	-136.3°	-142.5°	-148.7°
3	-131.3°	-136.5°	-142.5°	-148.7°
4	-131.2°	-136.5°	-142.5°	-148.7°
5	-131.2°	-136.5°	-142.5°	-148.7°

$f = 1\text{kHz}$ ,  $\Delta d = 1\text{S}$ ,  $\sigma d = 0$ ,  $\sigma_o = 5 \times 10^{-3} \text{ S/m}$ ,  $L = 1\text{km}$ .

For small values of  $\sigma d$  and  $\Delta d$ , we can obtain approximate expressions for  $c_0$  and  $c_1$ . From (42),  $c_1/c_0$  to lowest order is

$$\frac{c_1}{c_0} \approx \frac{-p_o}{\Omega_1} = \frac{-(\Delta d/2)\eta e^{-\gamma h}}{\frac{2}{1+e^{-2\Gamma_1 h}} + \sigma d K_1 e^{-\Gamma_1 h}} \quad (44)$$

where  $\eta = i\omega\mu_o/\gamma$ .

For small  $\sigma d$  and small  $|\Gamma_1| h$ , (44) reduces to

$$c_1/c_0 \approx -\Delta d \eta / 4 \quad . \quad (45)$$

For the same approximations in (39),  $c_0$  and  $c_1$  reduce to

$$c_0 \approx H_0, \quad c_1 \approx -\Delta d \eta H_0 / 4 \quad . \quad (46)$$

Thus  $c_0$  is approximately the homogeneous half-space value,  $H_0$ , and  $c_1$  is proportional to  $\Delta d$ .

#### 4.4 Vertical Magnetic Field

From (29) - (31), the vertical magnetic field  $H_z$  is given by

$$H_z = \begin{cases} -2 \sum_{n=1}^{\infty} \frac{\beta n}{\Gamma_n} [a_n e^{-\Gamma_n z} - b_n e^{\Gamma_n z}] \sin \beta n x & , \quad 0 < z < h \\ -2 \sum_{n=1}^{\infty} \frac{\beta n}{\Gamma_n} c_n e^{-\Gamma_n z} \sin \beta n x & , \quad z > h \end{cases} \quad (47)$$

The primary contribution to  $H_z$  comes from the  $n = 1$  term in the summation, and  $H_z$  can be approximated by

$$H_z \approx \begin{cases} \frac{-2\beta c_1 e^{-\Gamma_1 h}}{\Gamma_1} \frac{\cosh(\Gamma_1 z)}{\cosh(\Gamma_1 h)} \sin \beta x & , \quad 0 < z < h \\ \frac{-2\beta c_1}{\Gamma_1} e^{-\Gamma_1 z} \sin \beta x & , \quad z > h \end{cases} \quad (48)$$

It is easily seen that  $H_z$  is continuous at  $z = h$  and that the maximum  $|H_z|$  occurs at

$$x = \frac{\pi}{\beta} \left(m + \frac{1}{2}\right) = \frac{L}{2} \left(m + \frac{1}{2}\right) \quad , \quad (49)$$

where  $m$  is any integer.

The maximum value of  $|H_z|$  as a function of depth is shown in Figures 4 and 5. The maximum always occurs at  $z = h$ , and the field has exponential decay for  $z > h$  and  $\cosh(\Gamma_1 z)$  dependence for  $0 < z < h$ . The  $h$  dependence is shown in figure 4, and the frequency dependence is shown in Figure 5. The presence of a constant component ( $\sigma d \neq 0$ ) in the conducting layer always lowers the  $|H_z|$  values.

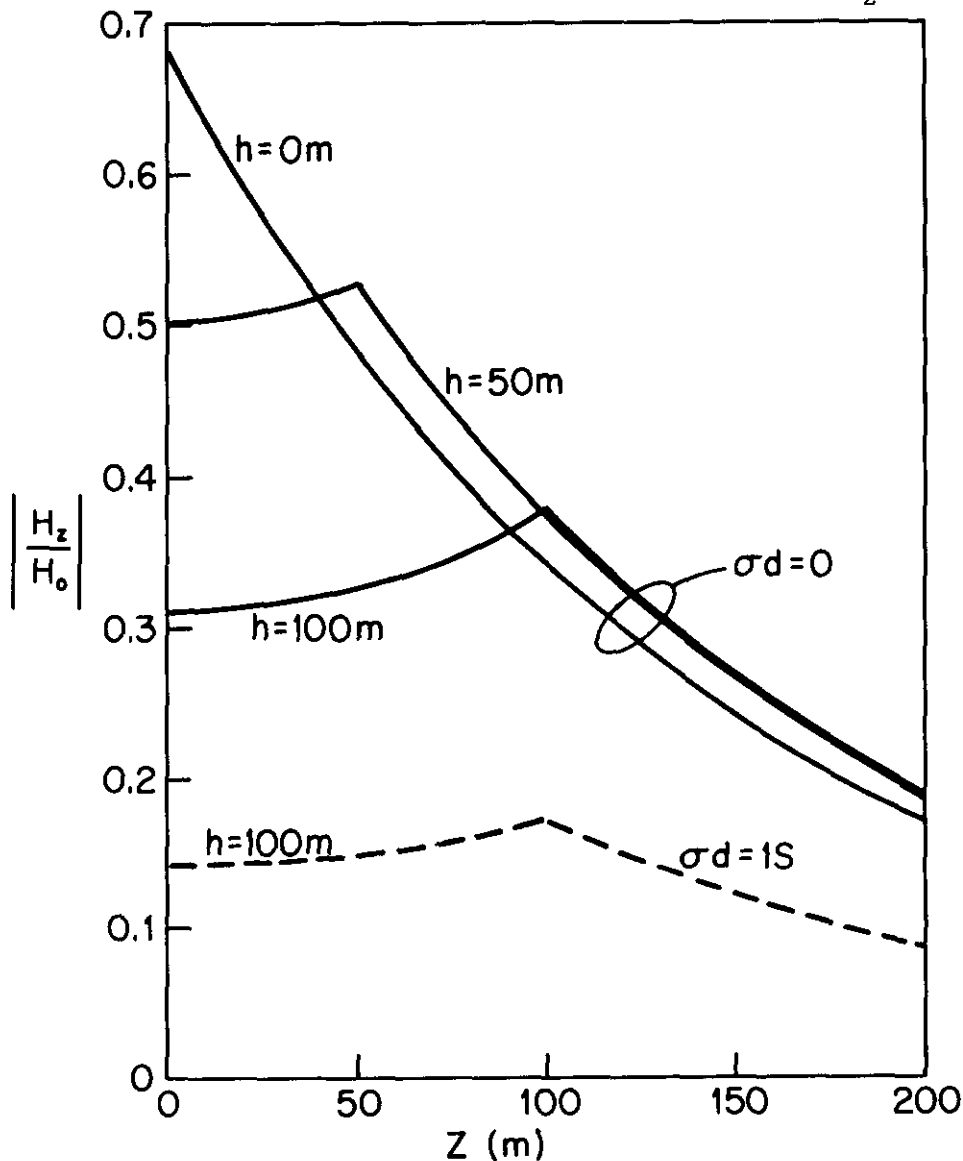


Figure 4. The maximum value of  $|H_z|$  versus depth for various layer depths. Parameters:  $f^z = 1 \text{ kHz}$ ,  $\Delta d = 1S$ ,  $\sigma_0 = 5 \times 10^3 \text{ s/m}$ , and  $L = 1 \text{ km}$ .

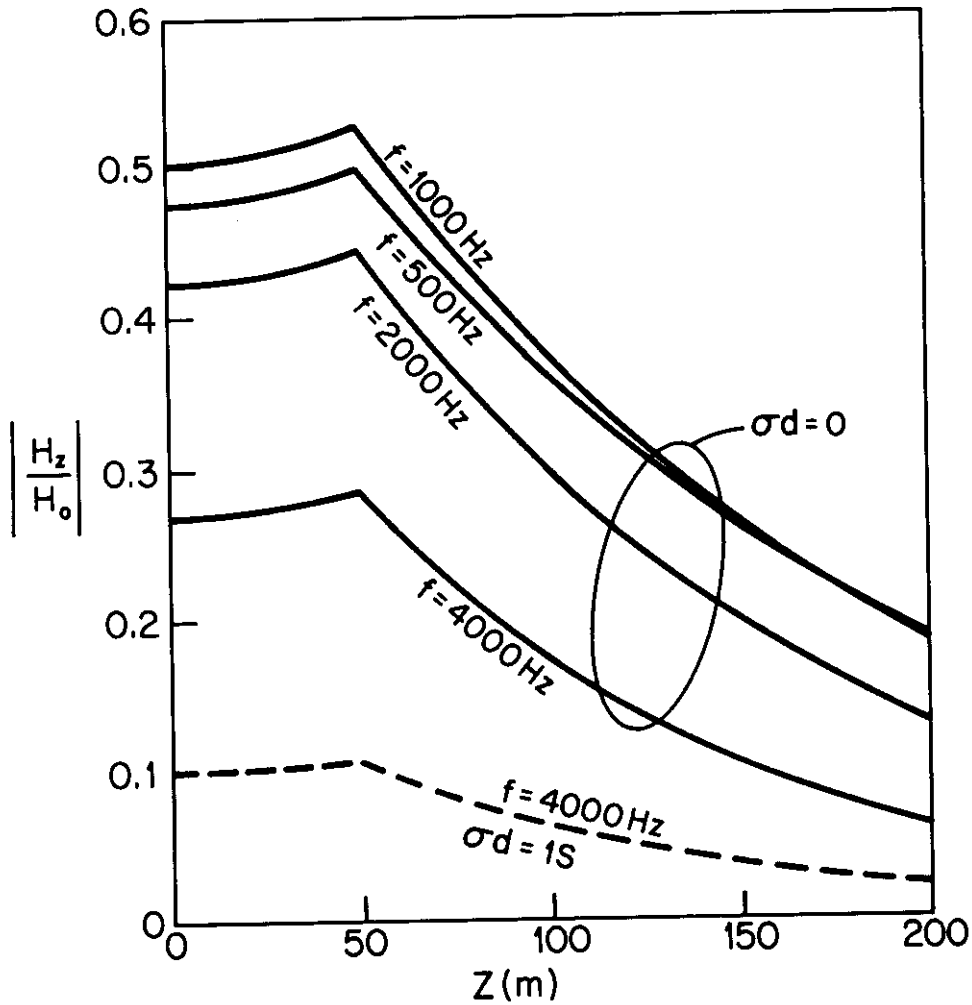


Figure 5. The maximum value of  $|H_z|$  versus depth for various frequencies. Parameters:  $h = 50$  m,  $\Delta d = 1S$ ,  $\sigma_o = 5 \times 10^{-3}$  S/m, and  $L = 1$  km.

A further approximation for  $H_z$  can be obtained from (46) and (48):

$$H_z \approx \frac{\beta \Delta d n H_o \sin \beta x}{2\Gamma_1} \cdot \begin{cases} \frac{\cos(\Gamma_1 z)}{\cos(\Gamma_1 h)} e^{-\Gamma_1 h} & , \quad 0 < z < h \\ e^{-\Gamma_1 z} & , \quad z > h \end{cases} \quad (50)$$

In addition, if  $|\Gamma_1| h$  and  $|\beta/\gamma|$  are small, (50) reduces to

$$H_z \approx \frac{\beta \Delta d H_o \sin \beta x}{2 \sigma_o} \begin{cases} 1 & , 0 < z < h \\ e^{-\gamma z} & , z > h \end{cases} . \quad (51)$$

#### 4.5 Surface Impedance

In many geophysical applications, the ratio of the orthogonal electric and magnetic fields tangential to the earth's surface is measured. This ratio is the surface impedance (Keller and Frischknecht, 1966) and is defined by

$$Z_s = E_y \Big|_{h=0} / H_o . \quad (52)$$

From (30) and (52),  $Z_s$  can be written

$$Z_s = - \sum_{n=0}^{\infty} (K_n / H_o) (a_n - b_n) \epsilon_n \cos(\beta n x) , \quad (53)$$

$$\text{where } \epsilon_n = \begin{cases} 1, & n=0 \\ 2, & n \neq 0 \end{cases}$$

and  $a_n$  and  $b_n$  are given by (34). Thus  $Z_s$  is even in  $x$ , and  $H_z$  is odd.

For the special case of  $\sigma d$  and  $\Delta d$  equal zero, (53) reduces to

$$Z_s = K_o = \eta . \quad (54)$$

This is just the intrinsic impedance of the half space.

#### 4.6 Conclusions

The effect of a thin conducting layer with lateral variation on the fields in a homogeneous half space has been analyzed. A vertical magnetic field is found to be generated, and its maximum value occurs at the layer depth as shown in Figures 4 and 5. The lateral dependence of  $H_z$  is approximately proportional to the derivative of the layer conductivity. Thus  $H_z$  is a good indicator of lateral variation of earth conductivity as has been noted previously in magneto-tellurics (Sims and Bostick, 1969; Word, et al., 1970).

Although the generation of vertical magnetic fields was of primary interest in this analysis, expressions were derived for all field components and for the surface impedance. This model is simpler than most models for volume irregularities because the thin sheet approximation allows an analytical solution whereas numerical solutions are generally required for inhomogeneous half-space geometries (Stodt, et al., 1981).

## 5. SCATTERING BY A BURIED CYLINDER

### 5.1 Introduction

In the previous two sections we examined the generation of vertical magnetic fields by periodic surface or volume irregularities. In this section we consider an infinitely long cylinder in an otherwise homogeneous half space. The cylinder could represent a man-made object such as a wire, rail, or pipe (Wait and Hill, 1974; Wait and Hill, 1977b) or a natural object such as a long ore body.

### 5.2 Formulation for the Fields

The geometry of the buried cylinder in a homogeneous half space is shown in Figure 6. The circular cylinder of radius  $a$  is centered at  $x = 0$  and  $z = h$ , the conductivity is  $\sigma_w$ , and the permeability is  $\mu_w$ . The half-space conductivity and permeability are  $\sigma_o$  and  $\mu_o$ , and the displacement currents are neglected.

As in the previous section, we assume that the tangential magnetic field at the surface is a constant (Wait and Spies, 1974):

$$H_x \Big|_{z=0} = H_o \quad (55)$$

The electric field outside the cylinder can be written in the following form

$$E_y = -H_o \eta e^{-\gamma z} - \frac{i\omega\mu_o I}{2\pi} [K_o(\gamma r) + K_o(\gamma \hat{r})] \quad (56)$$

where  $\eta = (i\omega\mu_o/\sigma_o)^{1/2}$  ,  $\gamma = (i\omega\mu_o\sigma_o)^{1/2}$  ,

$$r = [x^2 + (z-h)^2]^{1/2}, \quad \hat{r} = [x^2 + (z+h)^2]^{1/2} \quad ,$$

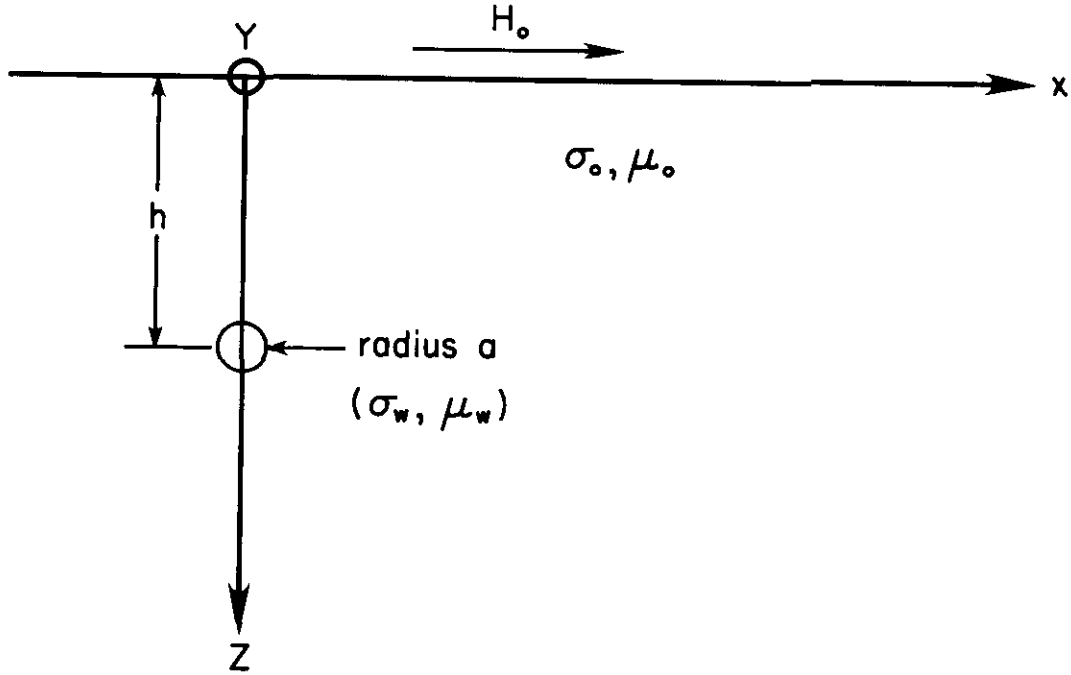


Figure 6. Geometry for a circular cylinder in a conducting half space.

and  $K_0$  is a modified Bessel function of first order (Abramowitz and Stegun, 1964). The longitudinal current  $I$  carried by the cylinder is unknown at this point. The first term in (56) represents the incident plane wave and the second term represents the field of the cylinder plus its image.

The horizontal magnetic field  $H_x$  is obtained by differentiating (56):

$$\begin{aligned}
 H_x &= \frac{1}{i\omega\mu_0} \frac{\partial E_y}{\partial z} \\
 &= H_0 e^{-\gamma z} + \frac{\gamma I}{2\pi} \left[ \frac{(z-h)K_1(\gamma r)}{r} + \frac{(z+h)K_1(\gamma \hat{r})}{\hat{r}} \right].
 \end{aligned} \tag{57}$$

It is easily seen from (57) that the boundary condition in (55) is satisfied. Also (57) has the proper  $r^{-1}$  singularity for small  $r$ .

The vertical magnetic field  $H_z$  is also obtained by differentiating (56):

$$\begin{aligned}
 H_z &= \frac{-1}{i\omega\mu_0} \frac{\partial E_y}{\partial x} \\
 &= \frac{-\gamma x I}{2\pi} \left[ \frac{K_1(\gamma r)}{r} + \frac{K_1(\gamma \hat{r})}{\hat{r}} \right].
 \end{aligned} \tag{58}$$

Thus  $H_z$  is zero in the absence of the cylinder ( $I=0$ ) and is also zero directly above or below the cylinder ( $x=0$ ).

A quantity of interest in magneto-tellurics (Keller and Frischknecht, 1966) is the surface impedance:

$$Z_s = -E_y \Big|_{z=0} / H_o \quad . \quad (59)$$

From (56),  $Z_s$  is given by

$$Z_s = \eta + \frac{i\omega\mu_o I}{\pi} K_o [\gamma(x^2 + h^2)^{1/2}] \quad . \quad (60)$$

The first term in (60) is the intrinsic impedance of the half space, and the second term is the cylinder contribution which is a maximum overhead ( $x=0$ ).

### 5.3 Derivation of the Cylinder Current

To obtain an expression for the current  $I$ , we apply the usual axial impedance condition at the edge of the cylinder (Wait and Hill, 1974):

$$\begin{aligned} Z_a I &= E_y \Big|_{r=a} \quad (61) \\ &= \frac{-i\omega\mu_o I}{2\pi} [K_o(\gamma a) + K_o(2\gamma h)] - H_o \eta e^{-\gamma h} \quad . \end{aligned}$$

Solution of (61) for  $I$  yields

$$I = \frac{-H_o \eta e^{-\gamma h}}{Z_a + \frac{i\omega\mu_o}{2\pi} [K_o(\gamma a) + K_o(2\gamma h)]} \quad . \quad (62)$$

The term involving  $K_o(2\gamma h)$  yields the interaction of the cylinder with the interface and has sometimes been neglected (Word, et al., 1970).

The explicit expression for the axial impedance  $Z_a$  is (Wait, 1959)

$$Z_a = \frac{i\omega\mu_w}{2\pi a\gamma_w} \frac{I_o(\gamma_w a)}{I_1(\gamma_w a)} \quad , \quad (63)$$



where  $\gamma_w = (i\omega\mu_w\sigma_w)^{1/2}$  and  $I_0$  and  $I_1$  are modified Bessel Functions (Abramowitz and Stegun, 1964). For small  $|\gamma a|$ , (63) reduces to

$$Z_a = \frac{1}{\pi\sigma_w a^2} \quad . \quad (64)$$

For large  $|\gamma_w a|$ , (63) reduces to

$$Z_a = \frac{i\omega\mu_w}{2\pi a\gamma_w} \quad . \quad (65)$$

#### 5.4 Numerical Results

A computer program was written for the current  $I$  as given by (62), for the vertical magnetic field  $H_z$  as given by (58), and for the surface impedance  $Z_s$  as given by (60). Results for  $|H_z/H_0|$  and  $|Z_s|$  are shown as a function of  $x$  in Figures 7-9. The curves are shown only for positive  $x$  because they are even in  $x$ . In each case the cylinder parameters are  $a = 2.5$  cm,  $\sigma_w = 10^6$  S/m, and  $\mu_w = 100\mu_0$  which could be representative of a rail or pipe.

In Figure 7 results are shown for the cylinder near the surface ( $h=2m$ ). At the surface,  $|H_z|$  peaks at about  $x = 2m$  whereas  $Z_s$  has a minimum directly overhead,  $x = 0$ . Physically the minimum in  $Z_s$  is caused by a "shorting out" of the horizontal electric field  $E_y$ . Also note that the peak in  $|H_z|$  corresponds to the maximum slope in  $|Z_s|$  as predicted by (58). For larger depths,  $|H_z|$  is seen to be much smaller and to peak at larger values of  $x$ .

In Figure 8, the cylinder is moved to a depth of 90m. At that depth, the cylinder has only a small effect on the surface impedance. However, a significant vertical magnetic field is still produced in the vicinity of the cylinder.

In Figure 9, surface results ( $z=0$ ) are shown for three frequencies. The decrease in  $H_z$  with frequency is due to the increase in the cylinder impedance  $Z_a$  which is predicted by the approximate expression in (65). This results in a decrease in cylinder current with increasing frequency. Again the peak in  $|H_z|$  and in the slope of  $|Z_s|$  occurs at about  $x = 2m$ .

#### 5.5 Conclusions

The simple model of a conducting cylinder in an otherwise homogeneous half space has been analyzed. The axial current carried by the cylinder produces

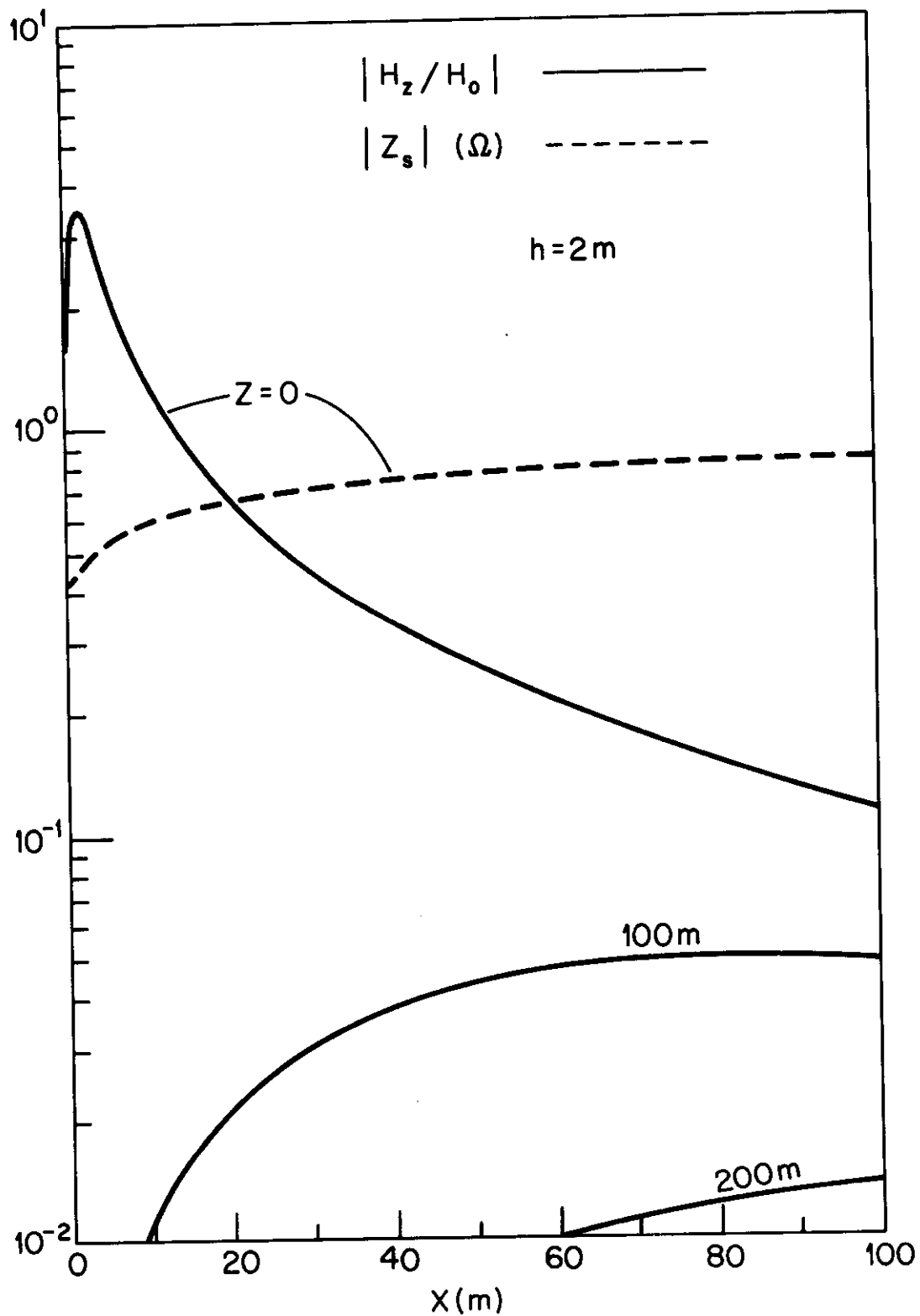


Figure 7. Vertical magnetic field and surface impedance for a cylinder near the surface. Parameters:  $a = 2.5$  cm,  $\sigma_w = 10^6$  S/m,  $\mu_w = 100 \mu_0$ ,  $h = 2$  m,  $\sigma = 10^{-2}$  S/m, and  $f = 1$  kHz.

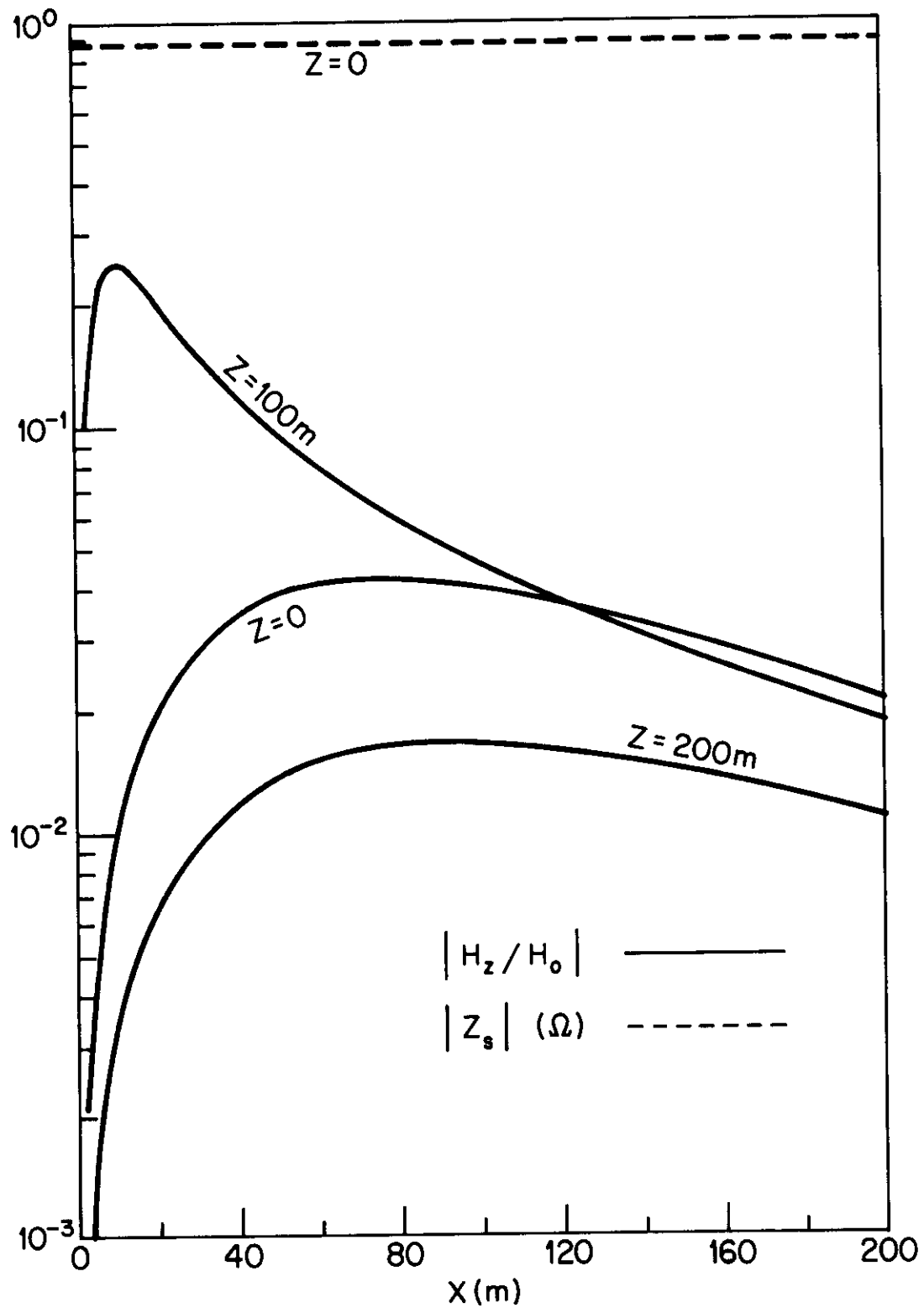


Figure 8. Vertical magnetic field and surface impedance for a cylinder at depth. Parameters: same as Figure 7 except that  $h = 90\text{m}$ .

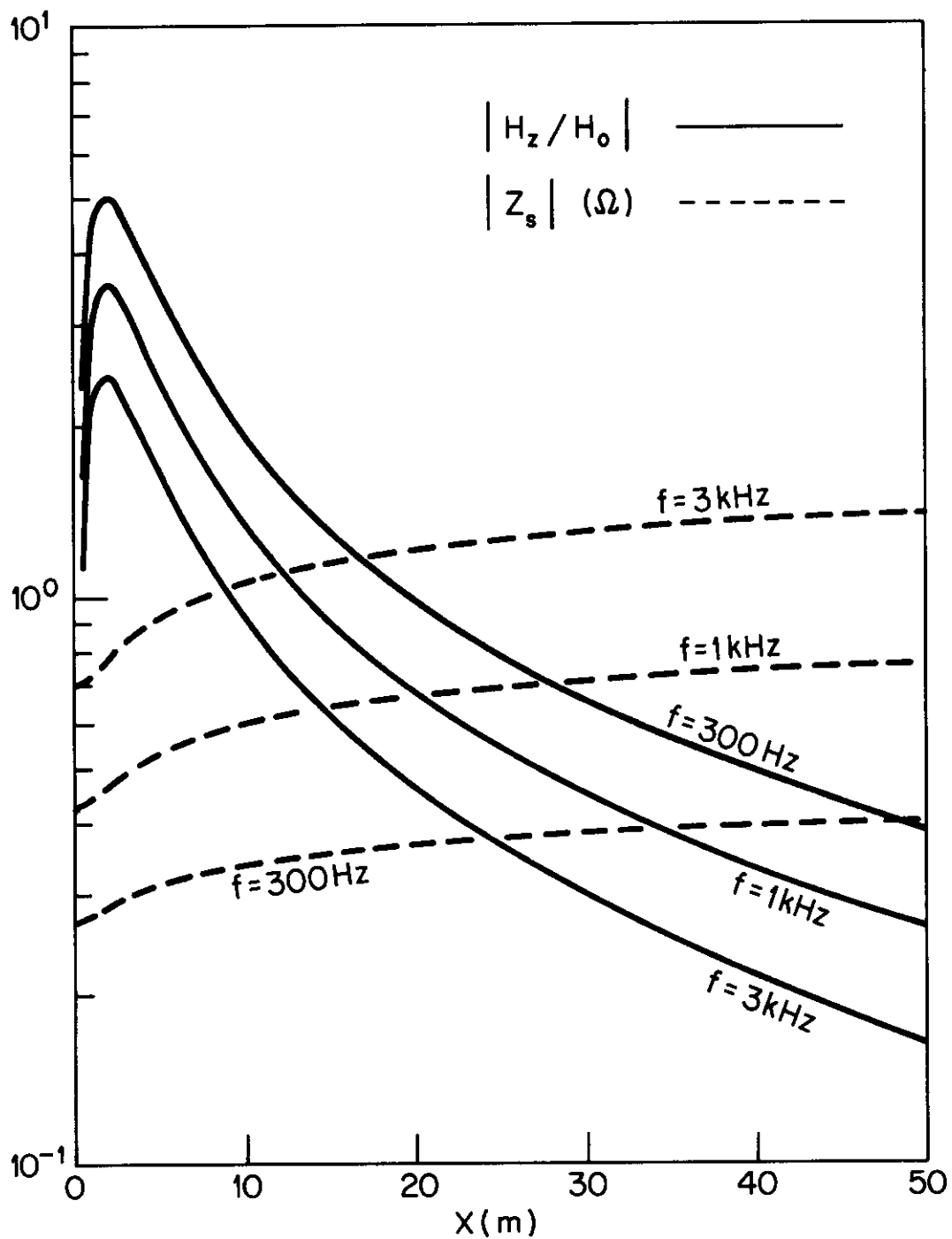


Figure 9. Frequency dependence for the vertical magnetic field and the surface impedance for a cylinder near the surface. Parameters:  $a = 2.5$  cm,  $\sigma_w = 10^6$  S/m,  $\mu_w = 100\mu_0$ ,  $h = 2$  m,  $\sigma = 10^{-2}$  S/m, and  $z = 0$ .

strong secondary electric and magnetic fields in the vicinity. The peak in the vertical magnetic field at the earth surface coincides with the maximum rate of change in the surface impedance. Numerical results have been presented both for a cylinder near the surface and at a large depth.

One logical extension would be to treat multiple cylinders in a half space in order to represent an ensemble of wires, pipes, rails, etc. The primary difference in the formulation would be that the axial impedance condition for the cylinder current in (61) would be replaced by a simultaneous set of equations involving all the cylinder currents (Wait, 1977). Also it is easy to modify the axial impedance of the cylinder as given by (63) to include a concentric dielectric layer to account for insulation or corrosion of the cylinder (Wait and Hill, 1977).

## 6. EFFECT OF A THIN CONDUCTING SHEET ON THE FIELDS OF A BURIED MAGNETIC DIPOLE

### 6.1 Introduction

The subject of transmitting from a buried magnetic dipole or small loop to the surface has been thoroughly studied with respect to mine communication and miner location (Wait, 1971a; Large, et al., 1973). Complications such as earth layering (Wait and Spies, 1971a; Wait and Spies, 1971b) and loop size and shape (Wait and Hill, 1980b) have also been analyzed. A recent attempt to infer earth conductivity from multi-frequency transmission at a large number of coal mines has indicated that a homogeneous half space is not a good earth model (Durkin, 1981). When a homogeneous half-space model is used to interpret the transmission data, the apparent earth conductivity generally decreases with both depth and frequency (Durkin, 1981).

Although it is possible to model the transmitted field using purely statistical theory (Lagace, et al., 1980), we attempt here to analyze an earth model which can explain the physics involved. Our model consists of a highly conducting thin sheet located over a homogeneous half space as shown in Figure 10. This is actually a special case of the thin sheet model considered in section 4 and can be obtained by setting both  $h$  and  $\Delta d$  equal to zero. Although we selected this thin sheet model primarily because it appears to fit the measured transmission data (Durkin, 1981), it actually has some further justification from earlier conductivity measurements which indicated an increased conductivity near the surface (Geyer, et al., 1974).

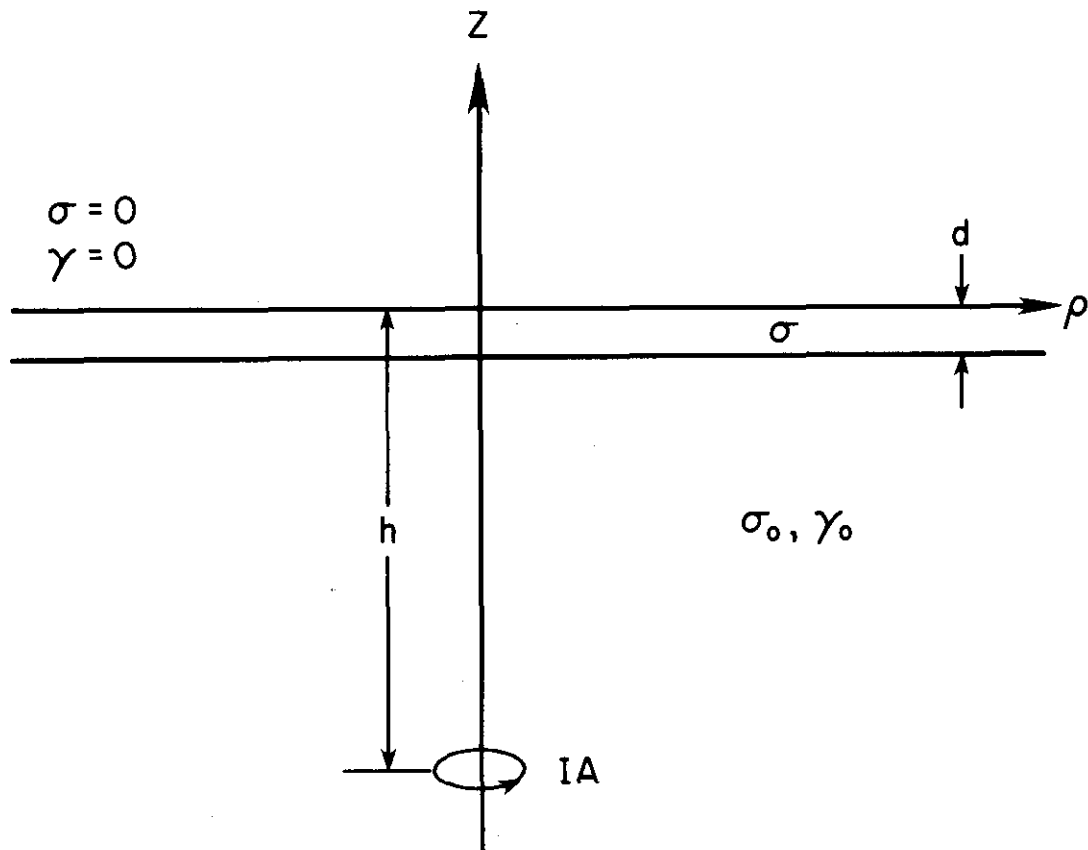


Figure 10. Geometry for a vertical magnetic dipole (small horizontal loop) in a conducting half space with a thin conducting sheet at the surface.

## 6.2 Formulation

The geometry for the thin sheet model and the buried vertical magnetic dipole source is shown in Figure 10. The half space has conductivity  $\sigma_0$ , and free space permeability  $\mu_0$  is assumed everywhere. The conducting sheet has a thickness  $d$  (which is small compared to the layer skin depth) and a conductivity-thickness product  $\sigma d$ . Displacement currents are neglected everywhere.

The vertical magnetic dipole source (small horizontal loop) has a moment  $IA$  and is located at  $z = -h$  on the  $z$  axis of a cylindrical coordinate system  $(\rho, \phi, z)$ . The fields can be derived from a magnetic Hertz vector with only a  $z$  component. In the half space,  $z < 0$ , the Hertz vector  $F_0$  satisfies the following Helmholtz equation everywhere except at the source

$$(\nabla^2 - \gamma_0^2) F_0 = 0 \quad , \quad (66)$$

$$\text{where } \gamma_0 = (i\omega\mu_0\sigma_0)^{1/2} \quad .$$

Above the half space,  $z > 0$ , the Hertz vector  $F_1$  satisfies Laplace's equation

$$\nabla^2 F_1 = 0 \quad . \quad (67)$$

In the half space, the fields are derived from  $F_0$  by (Wait and Spies, 1971)

$$H_{0\rho} = \frac{1}{i\omega\mu_0} \frac{\partial^2 F_0}{\partial\rho\partial z} \quad , \quad (68)$$

$$H_{0z} = \left( -\sigma_0 + \frac{1}{i\omega\mu_0} \frac{\partial^2}{\partial z^2} \right) F_0 \quad , \quad (69)$$

$$\text{and } E_{0\phi} = \frac{\partial F_0}{\partial\rho} \quad . \quad (70)$$

Above the half-space, the fields are derived from  $F_1$  by

$$H_{1\rho} = \frac{1}{i\omega\mu_0} \frac{\partial^2 F_1}{\partial\rho\partial z} \quad , \quad (71)$$

$$H_{1z} = \frac{1}{i\omega\mu_0} \frac{\partial^2 F_1}{\partial z^2} \quad , \quad (72)$$

$$\text{and } E_{1\phi} = \frac{\partial F_1}{\partial\rho} \quad . \quad (73)$$

The specific expressions for  $F_0$  and  $F_1$  are (Wait and Spies, 1971)

$$F_0 = \frac{i\omega\mu_0 IA}{4\pi} \int_0^\infty \frac{\lambda}{u_0} \left[ e^{-u_0|z+h|} + R(\lambda)e^{u_0 z} \right] J_0(\lambda\rho) d\lambda \quad (74)$$

and

$$F_1 = \frac{i\omega\mu_0 IA}{4\pi} \int_0^\infty T(\lambda)e^{-\lambda z} J_0(\lambda\rho) d\lambda \quad , \quad (75)$$

$$\text{where } u_0 = (\lambda^2 + \gamma_0^2)^{1/2}$$

and  $R(\lambda)$  and  $T(\lambda)$  are unknown.

The boundary conditions are that the tangential electric field is continuous at  $z = 0$  and that the tangential magnetic field is discontinuous by the amount of longitudinal current per unit length carried by the thin sheet:

$$(E_{o\phi} - E_{1\phi}) \Big|_{z=0} = 0 \quad (76)$$

and

$$(H_{1\rho} - H_{o\rho}) \Big|_{z=0} = \sigma d E_{1\phi} \Big|_{z=0} \quad (77)$$

By substituting the field expressions, (76) and (77) become

$$\frac{\lambda}{u_o} [e^{-u_o h} + R(\lambda)] - T(\lambda) = 0 \quad (78)$$

$$\frac{1}{i\omega\mu_o} [-\lambda T(\lambda) - \frac{\lambda}{u_o} (-u_o e^{-u_o h} + u_o R(\lambda))] = \sigma d T(\lambda) \quad (79)$$

Simultaneous solution of (78) and (79) yields

$$R(\lambda) = \frac{u_o - \lambda - i\omega\mu_o \sigma d}{u_o + \lambda + i\omega\mu_o \sigma d} e^{-u_o h} \quad (80)$$

$$T(\lambda) = \frac{2\lambda e^{-u_o h}}{u_o + \lambda + i\omega\mu_o \sigma d} \quad (81)$$

An interesting feature of the transmission coefficient  $T(\lambda)$  in (81) is that the dependence on  $\sigma d$  is algebraic rather than exponential. This type of algebraic dependence is typical of thin conducting sheets regardless of the geometry (Wait and Hill, 1977a).

### 6.3 Vertical Magnetic Field in Air

From (72), (75), and (81), the vertical magnetic field above the earth  $H_{1z}$  is given by



$$H_{1z} = \frac{IA}{2\pi} \int_0^{\infty} \frac{\lambda^3 e^{-u} h - \lambda z}{u_0 + \lambda + \omega \mu_0 \sigma d} J_0(\lambda \rho) d\lambda, \quad (82)$$

It is convenient to write  $H_{1z}$  in the following normalized form by setting  $g = \lambda h$  (Wait, 1971; Wait and Spies, 1971)

$$H_{1z} = \frac{IA}{2\pi h^3} Q, \quad (83)$$

where

$$Q = \int_0^{\infty} \frac{g^3 e^{-(g^2 + iH^2)^{1/2} - gZ}}{g + (g^2 + iH^2)^{1/2} + iHT} J_0(gD) dg, \quad (84)$$

$H = (\omega \mu_0 \sigma_0)^{1/2} h$ ,  $D = \rho/h$ ,  $Z = z/h$ , and  $T = \sigma d (\omega \mu_0 / \sigma_0)^{1/2}$ .  $Q$  is dimensionless and approaches unity as  $H$ ,  $Z$ , and  $D$  approach zero. It can be considered a correction to the field of a static magnetic dipole. For  $T$  equal to zero ( $\sigma d = 0$ ),  $Q$  in (83) reduces to the previous result for a homogeneous half space (Wait, 1971).

In general the integral in (84) must be evaluated numerically. The case of an observer at the surface ( $Z = 0$ ) directly above the source ( $D = 0$ ) is of particular interest, and numerical results for the magnitude of  $Q$  versus  $H$  are shown in Figures 11 and 12. The curves of  $|Q|$  versus  $H$  for fixed values of  $T$  in Figure 11 can be thought of as curves of  $|Q|$  versus depth  $h$  for fixed values of  $\omega$  and  $\sigma d$ . Note that  $Q$  approaches unity as  $H$  approaches zero regardless of the value of  $T$ . The curves of  $|Q|$  versus  $H$  for  $T$  proportional to  $H$  ( $T = \alpha H$ ) in Figure 12 can be thought of as curves of  $|Q|$  versus  $\omega$  for fixed values of  $h$  and  $\sigma d$ .

We present both formats for the variation of  $|Q|$  versus  $H$  because the variation of field strength with both depth and frequency are of particular interest in mine communication and miner location (Lagace, et al., 1980; Durkin, 1981). The results for  $T = 0$  in Figure 11 and for  $\alpha = 0$  in Figure 12 agree with previous results for the homogeneous half space (Wait, 1971).

#### 6.4 Apparent Earth Conductivity

Durkin (1981) has presented apparent earth conductivity data which is based on loop transmission data taken at a number of U.S. coal mines. The

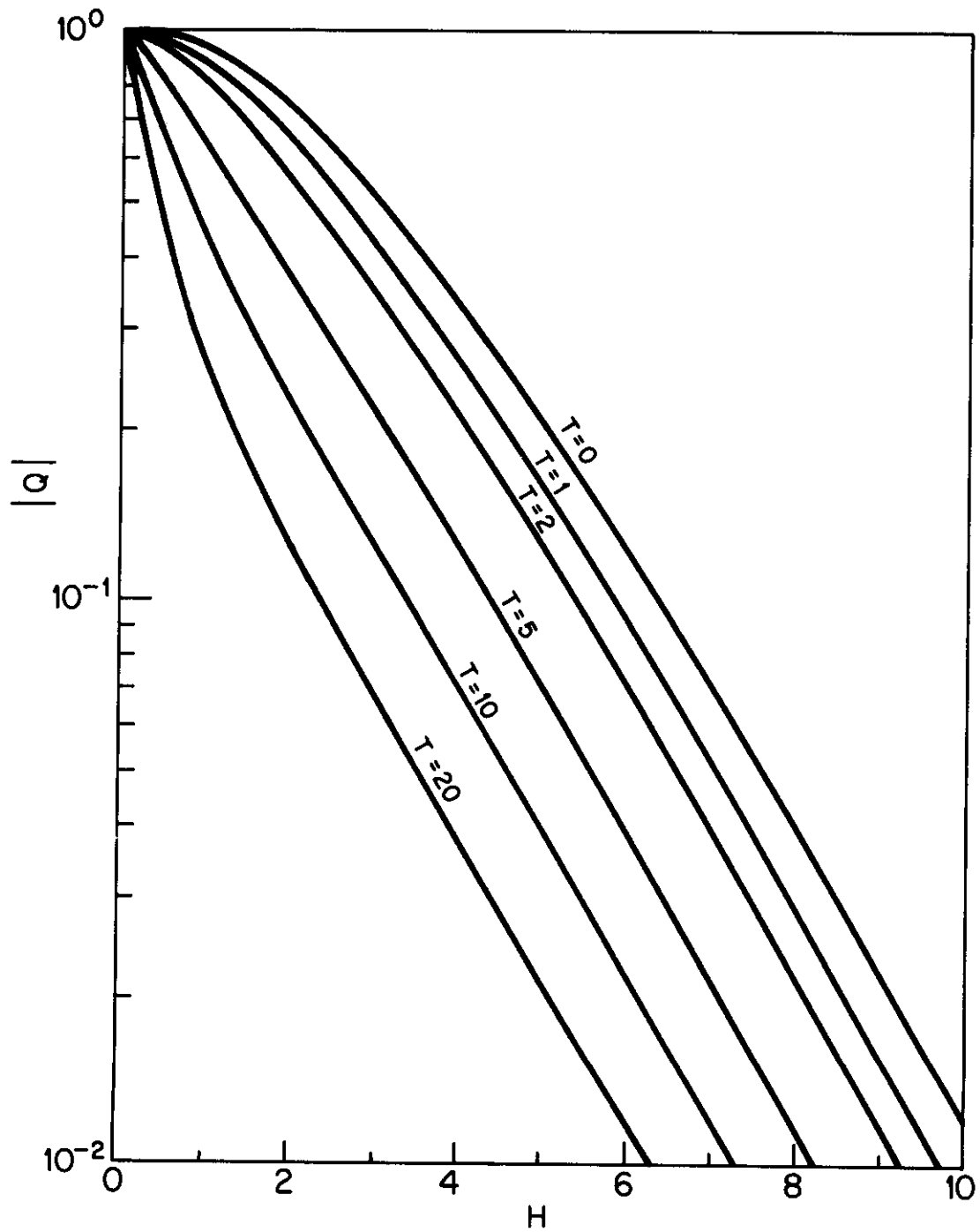


Figure 11. Magnitude of  $Q$  versus  $H$  for various values of  $T$ .

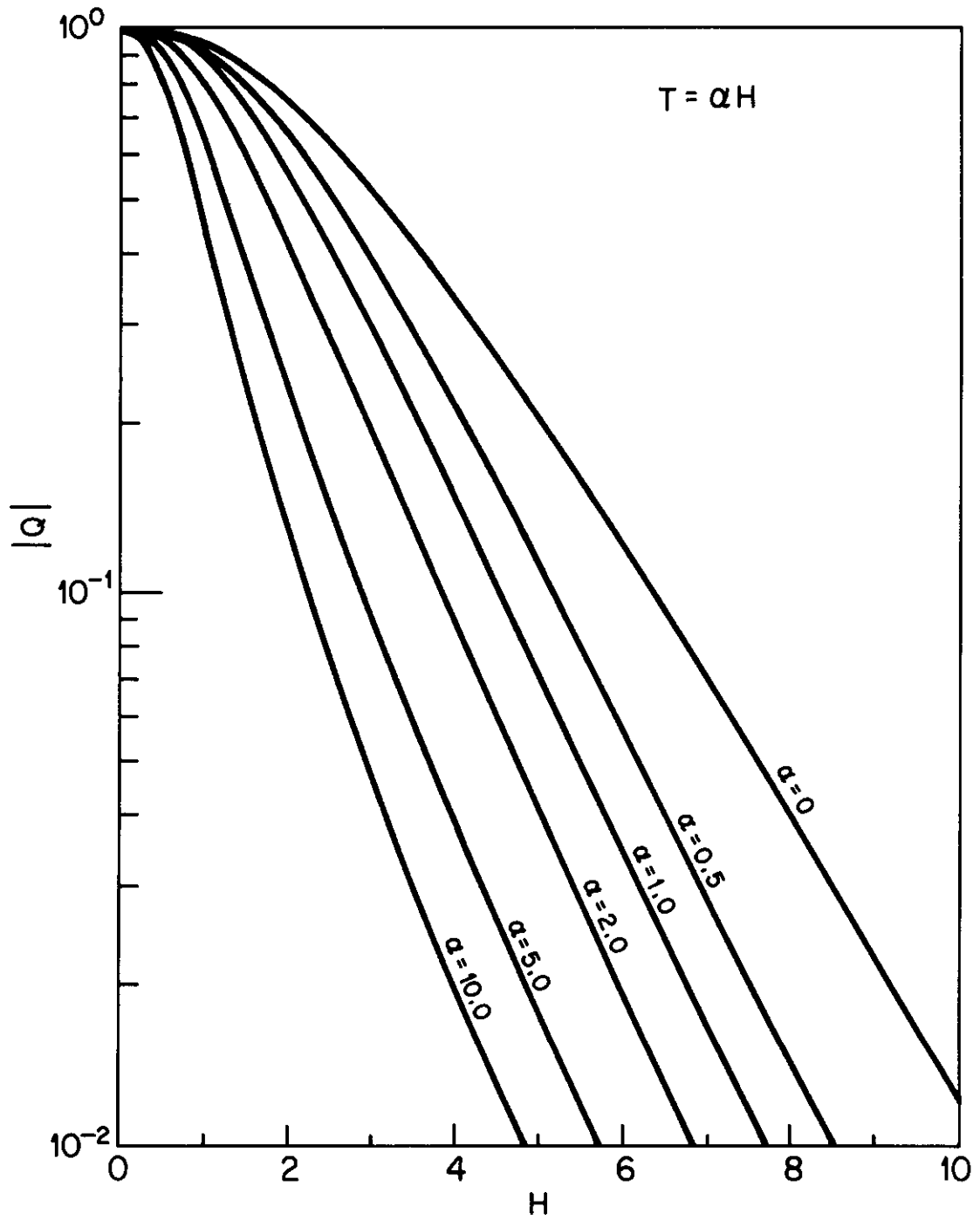


Figure 12. Magnitude of Q versus H for T proportional to H.  $T = \alpha H$ .

depths varied over a wide range, but were always known. Four transmission frequencies, 630, 1050, 1950, and 3030 Hz, were used at each site. By normalizing the data, it was possible to determine the value of  $|Q|$  from (83) for  $D = 0$ . Since  $|Q|$  has a monotonic decrease with  $H$ , it was possible to determine an apparent value  $H_a$  by assuming a homogeneous half space ( $T = 0$ ). From  $H_a$  an apparent conductivity value  $\sigma_a$  is simply

$$\sigma_a = H_a^2 / (\omega \mu_o h^2) \quad . \quad (85)$$

The surprising feature of the results was that  $\sigma_a$  tended to decrease with both depth and frequency.

Since measured rock conductivities (Parkhomenko, 1967) do not show a decrease with increasing frequency at ELF, it appears that the effect must be caused by the spatial conductivity variation. The thin sheet model which we have analyzed here is probably the simplest model which can predict both the depth and frequency effects.

To illustrate the effects, we can compute  $Q(H,T)$  for the actual values of  $\sigma_o$  and  $\sigma d$  and equate the magnitude of  $Q$  to that of a homogeneous half space ( $T = 0$ ):

$$|Q(H,T)| = |Q(H_a,0)| \quad (86)$$

The apparent conductivity is then determined from  $H_a$  by (85). Table 3 shows values of apparent conductivity determined from (85) and (86) for three depths at the four frequencies used in the Bureau of Mines measurements (Durkin, 1981). We assumed values of  $\sigma_o = 10^{-3}$  S/m and  $\sigma d = 10S$ . Note that the apparent conductivity decreases with both depth and frequency. Other calculations for different values of  $\sigma_o$  and  $\sigma d$  showed the same trends. Also shown in Table 3 are the mean values of apparent conductivity averaged over the various mine sites. Since the depths were different at each mine, the experimental mean values are roughly averaged over depth. Note that the experimental values tend to fall between our calculated values of  $h = 100$  m and 200 m.

Although our thin sheet model does predict the qualitative behavior of the experimental values, it does not quite predict the magnitude of decrease in apparent conductivity with frequency. However, an examination of raw data rather than mean values has shown that the depth behavior is easily predicted by the thin sheet model.

Table 3. Apparent conductivity,  $\sigma_a$  (S/m).  $\sigma d = 10S$  and  $\sigma_o = 10^{-3}$  S/m.

f \ h	100 m	200 m	400 m	Experimental Mean*
630 Hz	0.106	0.0544	0.0247	0.129
1050 Hz	0.105	0.0503	0.0213	0.0891
1950 Hz	0.101	0.0439	0.0173	0.0603
3030 Hz	0.094	0.0376	0.0145	0.0479

\*(Durkin, 1981)

### 6.5 Conclusions

The effect of a thin conducting sheet on the fields of a subsurface vertical magnetic dipole has been analyzed. The modification of the field expressions due to the conductivity thickness product  $\sigma d$  shows up only in the algebraic part of the reflection and transmission coefficients in (80) and (81). The particular effect on the vertical magnetic field at the surface is shown in Figures 11 and 12.

This earth model is particularly simple because it requires only two parameters, the earth conductivity  $\sigma_o$  and the conductivity thickness product  $\sigma d$ . Although more complicated layered or laterally inhomogeneous earth models could be analyzed, this simple thin sheet model is capable of at least qualitatively predicting the frequency and depth dependence of apparent conductivity deduced from transmission measurements (Durkin, 1981). Specific results are given in Table 3.

As far as modeling the true conductivity structure at operational coal mines, it may be that the thin sheet model is actually good for representing surface conductors, such as cables, pipes, etc., as well as increased surface conductivity (Geyer, et al., 1974). More detailed earth conductivity and transmission measurements would be required to obtain a more sophisticated knowledge of earth conductivity structure and of the effect of man-made conductors which can either enhance (Wait and Hill, 1975) or degrade transmission.

## 7. CONCLUSIONS AND RECOMMENDATIONS

This report consists primarily of a review of vertical magnetic noise, analyses of the conversion from horizontal to vertical magnetic noise, and an analysis of magnetic dipole transmission through a thin sheet model for the earth. Each section is self-contained and contains specific conclusions. In this section we present some general conclusions regarding noise and propagation models.

As far as the status of atmospheric noise at ELF and VLF, the thunderstorm sources are well known and well mapped (CCIR, 1964), and fairly good noise maps have been produced for VLF and ELF (Watt, 1967; Maxwell and Stone, 1965) by extrapolating downward in frequency from the CCIR atmospheric noise maps (CCIR, 1964). The main difficulty is that the past maps as well as ELF noise measurements for Project Sanguine (Wait, 1974) apply only to horizontal magnetic noise and not to the vertical component of interest. More recent vertical magnetic noise measurements by Westinghouse and the U.S. Bureau of Mines (Lagace, et al., 1980) provide a good beginning, but further measurements of both horizontal and vertical components both at the surface and at depth would be useful. Such noise measurements would help to understand the physics of vertical magnetic noise generation as well as enlarging the data base. Also, accompanying in situ earth conductivity measurements would provide further insight.

Three laterally inhomogeneous earth models were analyzed in sections 3-5. It was found that conversion from horizontal to vertical magnetic noise can be caused by rough surface scattering (section 3), volume scattering (section 4) or by long man-made conductors (section 5). For surface scattering, the vertical magnetic field will be strongest at the surface where the slope is maximum and will decay both above and below the surface. For volume scattering, the vertical magnetic field is strongest at volume irregularities and decays both above and below. In all cases, the lateral variation of surface impedance as measured in magneto-tellurics (Keller and Frischknecht, 1966) correlates strongly with the vertical magnetic field.

In section 6, an earth model with a thin conducting sheet was analyzed and was shown to agree at least qualitatively with the depth and frequency effects measured for magnetic dipole transmission (Durkin, 1981). The model is attractive because it contains only two parameters, earth conductivity and conductivity-thickness product of the layer, and because the calculations are no more difficult than those of the commonly used homogeneous half-space model.

The optimum goal of developing a single earth model to predict both the conversion from horizontal to vertical magnetic noise as well as the observed frequency and depth dependence of magnetic dipole transmission has not yet been reached. It is clear that lateral variation is necessary to predict the generation of vertical magnetic noise, but lateral variation may not be required to explain the transmission data as indicated in section 6. Probably a composite earth model containing both vertical and lateral variation could explain both the noise and transmission data. The simplest such model would be the inhomogeneous thin sheet which was analyzed in section 4 for plane wave incidence. It would be useful to analyze the same model for magnetic dipole transmission to see what effect the lateral variation has on transmission.

## 8. REFERENCES

- Abramowitz, M. and I. A. Stegun (1964), Handbook of Mathematical Functions, National Bureau of Standards, U.S. Government Printing Office, Washington, D.C.
- Adams, J.W., W.D. Bensema, and N.C. Tomoeda (1974), Surface magnetic field noise measurements at Geneva Mine, National Bureau of Standards, NBSIR 74-369, June.
- Barrick (1971), Theory of HF/VHF propagation across the rough sea, 1, 2, Radio Science, vol. 6, 517-533.
- Bensema, W.D. (1972), Coal mine ELF electromagnetic noise measurements, National Bureau of Standards Report 10-739, April.
- Bensema, W.D. (1977), A noise spectrum measurement system using the fast Fourier transform, IEEE Transactions on Electromag. Compat., vol. EMC-19, 37-43.
- CCIR (1964), Report 322, World Distribution and Characteristics of Atmospheric Radio Noise, International Telecommunications Union, Geneva.
- Chuang, S.L. and J.A. Kong (1981), Scattering of waves from periodic surfaces, Proc. IEEE, vol. 69, 1132-1144.
- Durkin, J. (1981), Study of through-the-earth transmission data as applied to earth conductivity, U.S. Bureau of Mines, Pittsburgh Mining and Safety Research Center.
- Geyer, R.G. (1972), The effect of dipping contact on the behavior of the electromagnetic field, Geophysics, vol. 37, 337-350.
- Geyer, R.G., G.V. Keller, and T. Ohya (1974), Research on the transmission of electromagnetic signals between mine workings and the surface, U.S. Bureau of Mines Open File Report 61-74, January.

- Hughes, W.J. and J.R. Wait (1975), Effective wave tilt and surface impedance over a laterally inhomogeneous two-layer earth, Radio Science, vol. 10, 1001-1008.
- Ishimaru, A. (1978), Wave Propagation and Scattering in Random Media, Vol. 2, Ch. 21, Academic Press, New York.
- Keller, G.V. and F.C. Frischknecht (1966), Electrical Methods in Geophysical Prospecting, Pergamon Press, Oxford.
- Lagace, R.L., J.M. Dobbie, T.E. Doerfler, W.S. Hawes, and R.S. Spencer (1980), Detection of trapped miner electromagnetic signals above coal mines, Final Report to U.S. Bureau of Mines (Contract # J0199037), July.
- Large, D.G., L. Ball, and A.J. Farstad (1973), Radio transmission to and from underground coal mines - theory and experiment, IEEE Trans. Comm., vol. COM-21, 194-202.
- Mann, J.E. (1964), Magnetotelluric theory of the sinusoidal interface, J. Geophys. Res., vol. 69, 3517-3524.
- Maxwell, E.L. (1967), Atmospheric noise from 20 Hz to 30 kHz, Radio Science, vol. 2, 637-644.
- Maxwell, E.L. and D.L. Stone (1963), Natural noise fields from 1 cps to 1 kc, IEEE Trans. Ant. Propagat., vol. AP-11, 339-343.
- Maxwell, E.L. and D.L. Stone (1965), 10 kc/s atmospheric noise predictions, DECO Electronics Report # 54-F-2, May.
- Millar, R.F. (1971), On the Rayleigh assumption in scattering by a periodic surface, Proc. Cambridge Phil. Soc., vol. 69, 217-225.
- Parkhomenko, E.I. (1967), Electrical Properties of Rock, Plenum Press, New York.
- Rankin, D. (1962), The magneto-telluric effect on a dike, Geophysics, vol. 27, 651-665.
- Reddy, I.K. and D. Rankin (1973), Magnetotelluric response of a two dimensional sloping contact by the finite element method, Pure and Applied Geophysics, vol. 105, 847-857.
- Rice, S.O. (1951), Reflection of electromagnetic waves from slightly rough surfaces, Comm. Pure Appl. Math., vol. 4, 351-378.
- Rosich, R.K. and J.R. Wait (1977), A general perturbation solution for reflection from two-dimensional periodic surfaces, Radio Science, vol. 12, 719-729.
- Sims, W.E. and F.X. Bostick (1969), Methods of magnetotelluric analysis, Electrical Geophysics Research Laboratory, University of Texas at Austin, Technical Report No. 58, January.
- Soderberg, E.G. (1981), ELF noise surveys, a review, NATO/AGARD Meeting of the Electromagnetic Wave Propagation Panel, Brussels, Belgium, 21-25 September.



- Stodt, J.A., G.W. Hohmann, and S.C. Ting (1981), The telluric-magenta-telluric method in two- and three- dimensional environments, Geophysics, vol. 46, 1137-1147.
- Strutt, J. W. (Lord Rayleigh) (1896), The Theory of Sound, vol. 2, 2nd ed., p. 89, Macmillan, New York.
- Wait, J.R. (1959), Electromagnetic Radiation from Cylindrical Structures, Pergamon Press, London.
- Wait, J.R. (1962), Electromagnetic Waves in Stratified Media, Pergamon Press, New York.
- Wait, J.R. (1971a), Criteria for locating an oscillating magnetic dipole buried in the earth, Proc. IEEE, vol. 59, 1033-1035.
- Wait, J.R. (1971b), Perturbation analysis for reflection from two-dimensional periodic sea waves, Radio Science, vol. 6, 387-391.
- Wait, J.R., Editor (1974), Special Issues on ELF communication, IEEE Trans. Comm., vol. COM-22, no. 4, 353-588, April.
- Wait, J.R. (1977), Excitation of an ensemble of parallel cables by an external dipole over a layered ground, AEU, vol. 31, 489-493.
- Wait, J.R. and D.A. Hill (1974), Guided electromagnetic waves along an axial conductor in a circular tunnel, IEEE Trans. Ant. Propagat., vol. AP-22, 627-639.
- Wait, J.R. and D.A. Hill (1975), Theory of the transmission of electromagnetic waves down a mine hoist, Radio Science, vol. 10, 625-632.
- Wait, J.R. and D.A. Hill (1977a), Electromagnetic shielding of sources within a metal-cased bore hole, IEEE Trans. Geoscience Electronics, vol. GE-15, 108-112.
- Wait, J.R. and D.A. Hill (1977b), Radio frequency transmission via a trolley wire in a tunnel with a rail return, IEEE Trans. Ant. Propagat., vol. AP-25, 248-253.
- Wait, J.R. and D.A. Hill (1980a), Electromagnetic fields in mine communi-environments, Final Report to U.S. Bureau of Mines (Contract No. J0199115), May.
- Wait, J.R. and D.A. Hill (1980b), Fields of a horizontal loop of arbitrary shape buried in a two-layer earth, Radio Science, vol. 15, 903-912.
- Wait, J.R. and K.P. Spies (1979a), Electromagnetic fields of a small loop buried in a stratified earth, IEEE Trans. Ant. Propagat., vol. AP-19, 717-718.
- Wait, J.R. and K.P. Spies (1971b), Evaluation of the surface electromagnetic fields for a buried magnetic dipole source, AFCRL Sci. Rept. No. 52, Contract No. PRO-Y-71-972, February.

- Wait, J.R. and K.P. Spies (1974), Magneto-telluric fields for a segmented overburden, J. Geomag. Geoelect., vol. 26, 449-458.
- Ward, S.H., J. O'Donnel, R. Rivera, G.W. Ware, and D.C. Fraser (1966), AFMAG-applications and limitations, Geophys., vol. XXXI, 576-605.
- Watt, A.D. (1967), VL Radio Engineering, Pergamon Press, Oxford.
- Word, D.R., H.W. Smith, and F.X. Bostick (1970), An investigation of the magnetotelluric tensor impedance method, Electrical Geophysics Research Laboratory, University of Texas at Austin, Technical Report No. 82, March.